

Backpressure control with predicted imminent saturation flow rate for urban networks

Dianchao Lin^a, Li Li^{b,*}

^a*School of Economics and Management, Fuzhou University, Fuzhou, Fujian, China*

^b*School of Civil Engineering, Fuzhou University, Fuzhou, Fujian, China*

Abstract

The network's admissible demand region (ADR), which is a key index to characterize a network's ability to handle incoming demands, is shaped by each movement's saturation flow rate (SFR). Existing backpressure (BP) traffic control policies commonly assumed a fixed and/or completely known SFR when calculating the pressure for decision-making. On one hand, since real-time traffic conditions can significantly influence the traffic supply, the fixed mean SFR (M-SFR) assumption could result in a mismatch between dynamic demand and supply. On the other hand, accurately predicting the imminent SFR (I-SFR) is challenging because of the complicated interactions between traffic participants. Hence, the completely known SFR assumption is impractical in real-world settings. Our paper demonstrates that, compared with only using the constant M-SFR information, using more knowledge of I-SFR can enlarge the upper bound of ADR. In addition, we theoretically prove that the BP with predicted I-SFR can guarantee network stability as long as the demand is interior to the ADR.

The proposed theory is validated by a calibrated simulation model in the experiments. Three I-SFR prediction methods with different accuracies are adopted: the M-SFR method, the heuristic estimation method, and the deep neural network method. They are tested in three BP-based control policies to investigate whether our findings are robust. The simulation results show that: a higher prediction accuracy of I-SFR can effectively help all three BP-based policies enlarge the network ADR, and more accurate I-SFR can productively reduce the average vehicle delay.

Keywords: Imminent saturation flow rate, backpressure, intersection control, urban networks, admissible demand region, capacity, Lyapunov optimization, neural network

1. Introduction

Intersections are the bottlenecks of the urban traffic network. The efficiencies at intersections significantly influence the efficiency of the overall network. Intersection management is mainly realized through traffic signal control. Based on the level of responsiveness to traffic, classical types of signalized intersection control include fixed-time, actuated, and real-time control. Over the last few decades, with the development of technology and the upgrade of the traffic control system, real-time control has received more and more attention in research and application (Dion and Hellinga, 2002; Christofa et al., 2013; Feng et al., 2015; Lin and Jabari, 2019, 2021). It requires the controller to sense the traffic conditions in real time and adapt the signal plan dynamically.

*Corresponding author, e-mail: lili@fzu.edu.cn

Compared with fixed-time and actuated controls, it can better match the traffic demand and supply and hence improve the intersection performance. Another typical classification method for intersection control is from the scale aspect, including isolated intersection control, arterial control, and network control. Among them, network control is the most challenging and meaningful because a problem in one part of a traffic network is sometimes best addressed by a decision at another location. Network control can be further classified into centralized and decentralized depending on whether there is a centralized controller to make decisions for the network. Usually, the centralized network control is not scalable and difficult to implement in real-world/real-time settings due to computational issues (Papageorgiou et al., 2003). For example, ACS-Lite (Gettman et al., 2007) can handle no more than 12 intersections in real time. To deal with the scalability and timeliness issues associated with network control optimization, decentralized network control techniques have been proposed and received much research attention in recent years.

Decentralized control algorithms can be solved quickly with small computing resources. To fully take this advantage, they usually combine with real-time control and adapt to fast-changing traffic status timely. Decentralized control algorithms (in real time) have short decision intervals (e.g., 10 s, 20 s). To obtain real-time traffic conditions, most decentralized control algorithms (theoretically) assume an information-rich traffic environment with the help of new technologies such as video camera recognition and connected vehicle communication. Different information is then extracted from the real-time monitored traffic condition to feed the algorithms. Typical examples of decentralized control algorithms include heuristic approaches using expected traffic demand information at the intersection in the next cycle (Smith, 1980; Lämmer and Helbing, 2008, 2010; Smith, 2011), backpressure (BP) based approaches using the queue sizes information along the intersection arcs in both upstream and downstream approaches (Wongpiromsarn et al., 2012; Varaiya, 2013), and other approaches using the expected outflow rates (Noaeen et al., 2021) or upstream traffic conditions (De Gier et al., 2011).

Among all the decentralized traffic control approaches, BP-based policies received lots of attention in the last decade. They were originally proposed in a communication network to solve the packet transmission problem (Tassiulas and Ephremides, 1992), and were later introduced to traffic network by Wongpiromsarn et al. (2012) and Varaiya (2013) independently. Since then, BP-based policies have experienced continuous improvements to make them more tailored for traffic problems (Xiao et al., 2014; Le et al., 2015, 2017; Chai et al., 2017; Hao et al., 2019; Li and Jabari, 2019; Mercader et al., 2020). A detailed review about the development of BP in traffic signal timing can be found in Levin (2023). BP-based techniques have two key features that make them attractive for intersection control. The first is that they do not require prior knowledge of demands. The second is that while they are decentralized (applied at the isolated intersection level), they come with provable guarantees of stability at the network level and maximize the network's throughput. Like many other decentralized network control algorithms, BP-based policies usually divide time into small (equal) intervals. Each intersection makes control decisions independently using the neighboring information at the beginning of each interval. In the original BP policy (e.g., Varaiya (2013)), the controller collects the real-time vehicular queue lengths of different movements and calculates the pressure of each movement based on its demand (queue length and turning ratios) and supply (saturation flow rate, SFR). The phase (a combination of non-conflicting movements) with the maximum total movement pressure is then activated during this interval. Extensions to BP include various aspects, such as a cyclic BP, which has a fixed phase sequence and predetermined cycle length (Kouvelas et al., 2014; Le et al., 2015; Sun and Yin, 2018; Levin et al., 2020; Robbennolt et al., 2022; Barman and Levin, 2022), a position-weighted BP (PWBP) that assigns weights to vehicles based on their distance to the intersection so as to discharge more urgent vehicles (Li and Jabari, 2019, 2020), a switching-curve-based BP (SCBP) that

considers the phase switching loss (at the start-up of green) to reduce the switching frequency of high demand (Wang et al., 2022), and a delay-based BP that considers vehicle delay instead of queue length when calculating the pressure (Liu and Gayah, 2022, 2023; Dixit et al., 2020). Many researchers have also considered more complicated scenarios with pedestrians (Chen et al., 2020), transit (Xu et al., 2022), automated vehicles (Rey and Levin, 2019), and non-connected vehicles (Gregoire et al., 2014a; Xiao et al., 2015a,b; Li et al., 2021) to make BP more suitable for practice.

A critical step in establishing the network’s stability guarantee and throughput maximization of BP-based policies is defining the admissible demand region (ADR, also named the capacity region) of the network (including traffic network, communication network, etc.) (Tassiulas and Ephremides, 1992; Neely, 2010; Varaiya, 2013). This is the set of arrival rates to the network that can be accommodated by an available stabilizing control policy under given technique background so that the queue length will be finite with a probability of 1. Arrival rates outside of the ADR typically cannot be accommodated by any control policy and lead, if they persist, to network-wide congestion (Li and Jabari, 2019). The size of a network’s ADR is determined by network structure, SFR (the supply ability), and available control policies. It characterizes the network’s ability to carry incoming demands. Despite that studies about the communication network usually use changeable SFR (Neely, 2010), when it comes to the traffic network, most researchers used to assume a fixed SFR when formulating the BP models (Le et al., 2015; Gregoire et al., 2014b; Zaidi et al., 2015; Gregoire et al., 2016; Rey and Levin, 2019; Wei et al., 2019; Levin et al., 2020; Chen et al., 2020; Tsitsokas et al., 2021; Xu et al., 2022; Wang et al., 2022). This is because, in conventional traffic environments, the changing SFR can hardly be obtained in real time due to technical limitations. Traffic engineers usually only know the mean SFR (M-SFR) through historical data. Therefore, the M-SFR is commonly used for signal timing in conventional traffic controls. Despite technological advances, the custom of using M-SFR in traffic controls has continued even when an information-rich traffic environment is assumed. As SFR can influence capacity (Zhao et al., 2018) and shape the ADR, we have to realize that using a fixed M-SFR and a changeable SFR will lead to different sizes of ADR.

Fig. 1 shows an example of why a movement’s SFR may vary a lot in real time. Although the demands of northbound movement in Fig. 1(a) and Fig. 1(b) are the same, their real-time supplies should be completely different. Clearly, when discharging, queues in Fig. 1(a) will repeatedly move and stop, while vehicles in Fig. 1(b) will pass smoothly. That is because urban road network not only serves passing automobiles but also serves other types of traffic (e.g., non-motorized vehicles, pedestrians) and automobiles with other purposes (e.g., parking vehicles, slowing-down vehicles for visiting and shopping). The interactions between different traffic participants inevitably influence the automobiles’ passing efficiency. In addition, features of the passing automobiles, such as vehicle compositions (e.g., cars, buses, heavy vehicles) and driver characteristics (e.g., aggressive or not), will also interfere with the passing efficiency. As a result, the continuously changing real-time traffic conditions unavoidably lead to fluctuating SFRs for different intervals. In an information-rich traffic environment such as a connected environment that is usually assumed by BP-based policies, predicting/estimating such dynamic SFR in real time becomes possible and achievable (though not simple) (Wang et al., 2020). Unfortunately, as stated above, most BP-related traffic control research still used a constant M-SFR when computing the pressure for each movement and assumed a fixed ADR. Although a few BP studies realized the randomness in SFR (Varaiya, 2013; Zaidi et al., 2016; Le et al., 2017; Wu et al., 2017; Hao et al., 2019; Mercader et al., 2020; Du and Kouvelas, 2022), they simply assumed the stochastic SFR could be completely known and neglected the importance of prediction. Some other research modeled the supplies as dynamic movement fluxes with an assumption of 100% accurate assessment (Li and Jabari, 2019), or estimated the SFR using measured values from detectors (Xiao et al., 2015a,b). However,

there were no discussions about the possible changes in associated ADR compared with using a fixed M-SFR. In addition, when we only have partial dynamic SFR information (with a prediction accuracy of less than 100%), the impacts on ADR and network performance are still unknown.

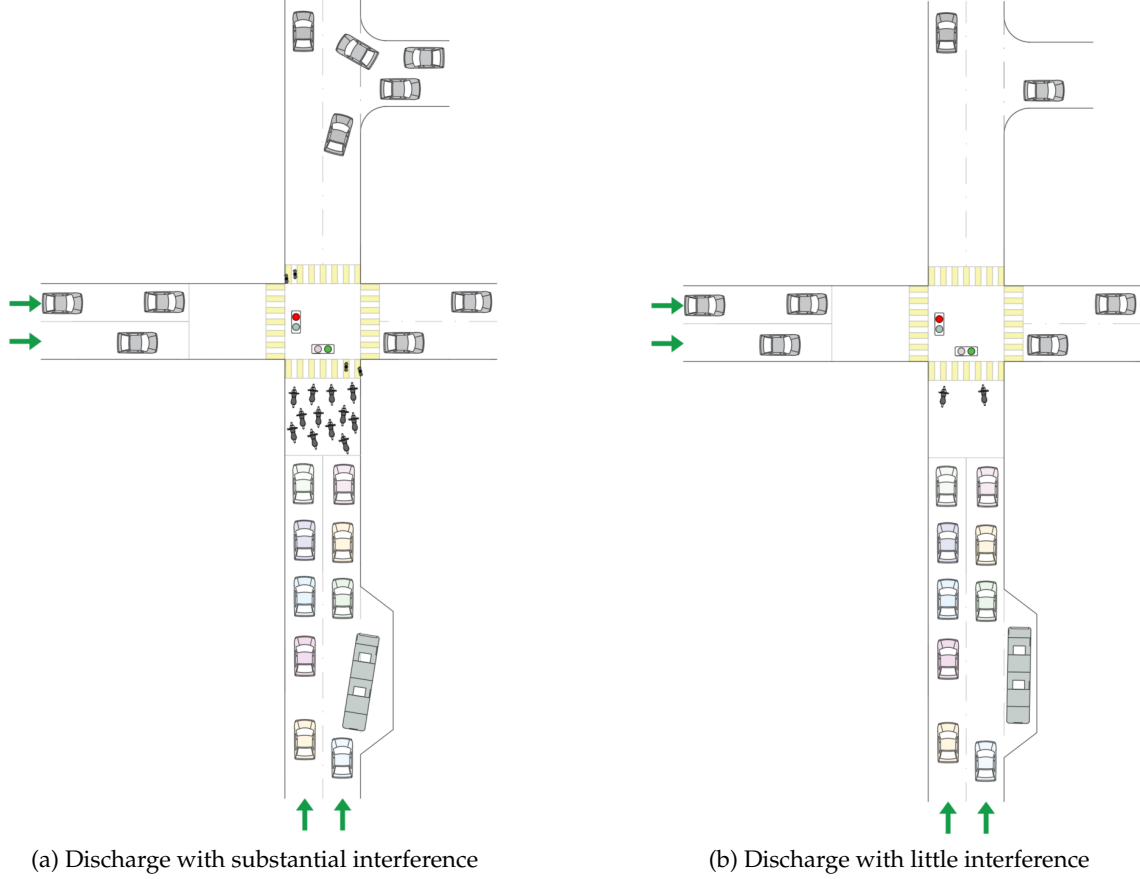


Fig. 1: Two types of “supply ability” for the northbound automobiles in real time

In this paper, we no longer assume the movement supply to be fixed and/or completely known. Instead, when computing the movement pressure, we consider the *imminent SFR* (I-SFR) defined by the SFR of the next time interval. That is, at any decision moment, a movement’s I-SFR refers to its real-time SFR that is about to be achieved if it receives green next interval. We assume the controller can predict the I-SFR to some degree and investigate the influence of I-SFR’s knowledge level on the network’s ADR and other performances. The main contributions of this paper are twofold:

- We characterize the relationship between ADR and the knowledge level of I-SFR with theoretical proof.
- We replace the fixed/known SFR in BP control with a predicted I-SFR and rigorously prove the stability of the extended BP when the arrival rate is interior to the corresponding ADR.

The remainder of this paper is organized as follows: [Sec. 2](#) describes the traffic dynamics model, formally defines ADR, and demonstrates some representative BP models. [Sec. 3](#) systematically deduces the relationship between ADR and SFR, and characterizes the changes in ADR with different I-SFR knowledge levels. [Sec. 4](#) proposes the BP with predicted I-SFR and rigorously

demonstrates the network-wide stability properties of the new BP approach using the Lyapunov drift technique. Sec. 5 shows the simulation results, and Sec. 6 concludes the paper.

2. Problem description

2.1. Notation

Consider an urban traffic network $(\mathcal{N}, \mathcal{L})$, where \mathcal{N} is a set of network nodes representing intersections, and $\mathcal{L} \subset \mathcal{N} \times \mathcal{N}$ is a set of directed links representing road segments. A movement is defined as a tuple composed of the origin and destination links. A movement i is defined as movement m 's upstream movement when i 's destination link is m 's origin link. Similarly, j is defined as m 's downstream movement when j 's origin link is m 's destination link. As shown in Fig. 2, we denote by $U(m)$ the set of m 's all upstream movements and by $O(m)$ the set of m 's all downstream movements.

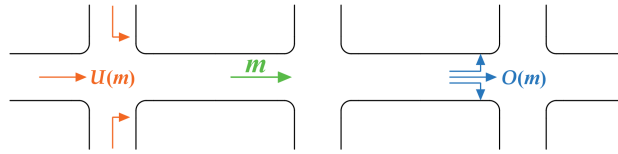


Fig. 2: Movement m 's upstream and downstream movements

For each node $n \in \mathcal{N}$, let \mathcal{M}_n denote the set of allowed movements between its inbound and outbound links. A movement $m \in \mathcal{M}_n$ when its origin link is an inbound link of n and its destination link is an outbound link of n . The set of all network movements is denoted by $\mathcal{M} \equiv \mathcal{M}_1 \sqcup \dots \sqcup \mathcal{M}_{|\mathcal{N}|}$, and $|\mathcal{M}|$ is the size of \mathcal{M} (the total number of movements in the network). A signal phase consists of junction movements that do not conflict with one another. We denote by Φ_n the set of allowable intersection phases at n and by $\Phi \equiv \times_{n \in \mathcal{N}} \Phi_n$ the set of allowable network phasing schemes. Usually, an allowable phase does not allow crossing conflicts and only allow merging conflicts between a protected and a permitted movement. Example allowable phases for a four-legged intersection are shown in Fig. 3 (right-turns are controlled).

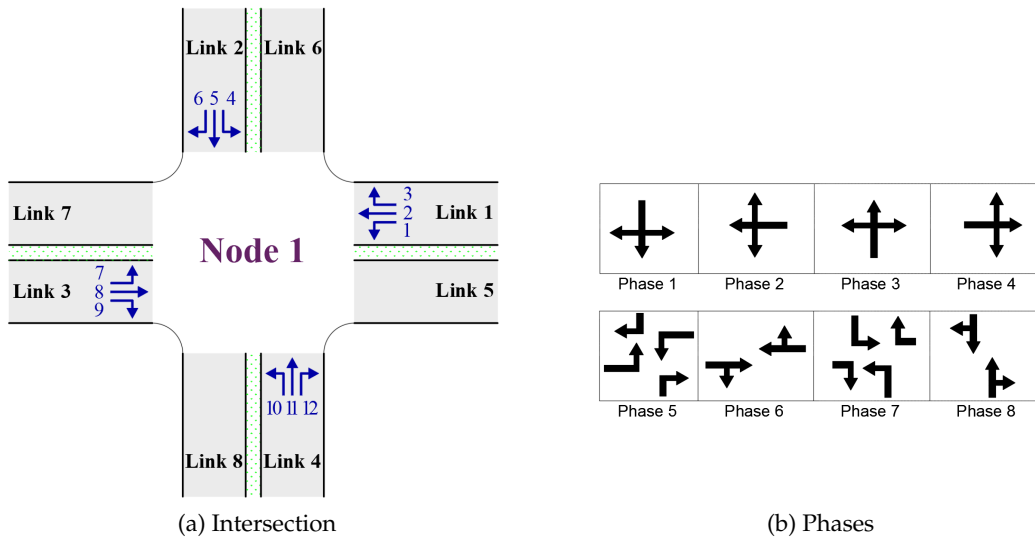


Fig. 3: An example of a four-legged intersection and its allowable phase set

2.2. Demand and queueing dynamics

We discretize time into intervals of equal length and use time t to refer to the beginning of interval $[t, t+1)$. For any $m \in \mathcal{M}$, let $a_m(t)$ denote its exogenous arrivals during $[t, t+1)$, and let $x_m(t)$ denote its queue length at time t . $\mathbf{X}(t) = \{x_m(t)\}$ is the queue length array of all the movements within the network. Assume phase $\Phi \in \Phi$ is selected for interval $[t, t+1)$, we let $\phi_m(t)$ denote m 's passing status during $[t, t+1)$, which equals 1 if passing is allowed, and 0 otherwise. Take Fig. 3 for example: for Node 1, when $\Phi_1 = \text{"Phase 2"}$ for $[t, t+1)$, we have that $\phi_m(t) = 1$ for $m \in \{1, 2, 3\}$, and $\phi_m(t) = 0$ for $m \in \{4, 5, \dots, 12\}$. Let $s_m(t)$ denote m 's I-SFR during $[t, t+1)$, and $r_m(t)$ denote the proportion of all vehicles from m 's upstream movements $U(m)$ that will directly join movement m at time t . Note that for any $m \in \mathcal{M}$, there is $\sum_{j \in O(m)} r_j(t) \leq 1$ ¹.

Given a movement m in the network, its demand arrivals during $[t, t+1)$ (denoted by $\lambda_m(t)$) is given by

$$\lambda_m(t) = a_m(t) + r_m(t) \sum_{i \in U(m)} q_i(t, \Phi), \quad (1)$$

where $q_i(t, \Phi)$ is real-time number of departures:

$$q_i(t, \Phi) = \min[x_i(t), s_i(t)\phi_i(t)].^2 \quad (2)$$

Note that for a single intersection, (1) reduces to $\lambda_m(t) = a_m(t)$ since no upstream movements exist.

The queueing dynamic of each movement m follows

$$x_m(t+1) = \max[x_m(t) - s_m(t)\phi_m(t), 0] + \lambda_m(t). \quad (3)$$

Let λ_m denote m 's average/expected arrival rate, and c_m denote m 's average/expected service rate (capacity). In the traffic system, arrivals and departures satisfy the law of large numbers, and we do not distinguish their "average value" and "expectation", i.e., $\lambda_m = \lim_{T \rightarrow \infty} \frac{1}{T} \sum_{t=0}^{T-1} \lambda_m(t) = \mathbb{E}\{\lambda_m(t)\}$, $c_m = \lim_{T \rightarrow \infty} \frac{1}{T} \sum_{t=0}^{T-1} s_m(t)\phi_m(t) = \mathbb{E}\{s_m(t)\phi_m(t)\}$.

Definition 1 (Rate stability). A movement m is rate stable if (Neely, 2010, Definition 2.2):

$$\lim_{t \rightarrow \infty} \frac{x_m(t)}{t} = 0 \quad \text{with probability 1.} \quad (4)$$

Theorem 1. A movement m is rate stable if and only if $\lambda_m \leq c_m$ (Neely, 2010, Theorem 2.4 a).

Rate stability says that a network is stable if and only if the arrival rate is no larger than the capacity for each movement. Considering that the actual departure rate cannot exceed the arrival rate, one can easily conclude that if a movement m is stable, its average/expected departure rate would be equal to its average arrival rate in the long run, i.e., $\mathbb{E}\{q_m(t)\} = \lambda_m$.

Let a_m denote the average exogenous arrival rate of m , and r_m denote the average turning ratio of m . As $q_i(t)$ and $r_m(t)$ are independent, taking an expectation on both sides of (1) yields

$$\lambda_m = a_m + r_m \sum_{i \in U(m)} \lambda_i. \quad (5)$$

¹ $\sum_{j \in O(m)} r_j(t) < 1$ only when there is exiting traffic in the midway of links.

²Here we assume that all vehicles on the link can pass the intersection within a one-time step. When the link is too long, it can be divided into several links. These links can be connected with a virtual junction with only one always green phase (Varaiya, 2013).

As $a_m = \lambda_m - r_m \sum_{i \in U(m)} \lambda_i$, we have

$$\mathbf{a} = (\mathbf{I} - \mathbf{R}) \cdot \boldsymbol{\lambda}, \quad (6)$$

where $\mathbf{a} = \begin{pmatrix} a_1 \\ \vdots \\ a_{|\mathcal{M}|} \end{pmatrix}$ is the exogenous-arrival-rate vector, $\boldsymbol{\lambda} = \begin{pmatrix} \lambda_1 \\ \vdots \\ \lambda_{|\mathcal{M}|} \end{pmatrix}$ is the demand rate vector, \mathbf{I} is an identity matrix, and \mathbf{R} is a $|\mathcal{M}| \times |\mathcal{M}|$ turning ratio matrix, whose locations of non-zero values are decided by the network structure. Note that for any traffic network, if the average exogenous arrival rates are all zeros ($\mathbf{a} = \mathbf{0}$), the average demand rates will also be zeros ($\boldsymbol{\lambda} = \mathbf{0}$). Hence, $(\mathbf{I} - \mathbf{R})$ must be invertible in traffic network, and we have $\boldsymbol{\lambda} = (\mathbf{I} - \mathbf{R})^{-1} \cdot \mathbf{a}$.

Definition 2 (Admissible demand region, ADR). The ADR, denoted by \mathcal{D} , is defined as the closure, i.e., the convex hull, of the set of all demand rate vectors $\boldsymbol{\lambda} \in \mathbb{R}_{|\mathcal{M}|}^+$ for which there exists a stabilizing control policy under given technique background.

Clearly, if a demand vector lies in ADR, then there exists a control policy with which all movements in the network satisfy rate stability. Furthermore, the expressions of demand rates for a single intersection and a network (with more than one intersection) are slightly different.

Remark 1. For a single intersection, \mathbf{R} is a zero matrix and $\boldsymbol{\lambda} = \mathbf{a}$, hence \mathcal{D} defines the convex hull of all possible exogenous-arrival-rate vectors \mathbf{a} for which there exists a stabilizing control policy.

Remark 2. For a network, $\boldsymbol{\lambda} = (\mathbf{I} - \mathbf{R})^{-1} \cdot \mathbf{a}$, hence \mathcal{D} defines the convex hull of all combinations of exogenous-arrival-rate vectors and turning ratio matrix (\mathbf{a}, \mathbf{R}) for which there exists a stabilizing control policy. In this paper, we assume that the vehicle routing is predetermined by the drivers and cannot be optimized through a control policy.

2.3. Backpressure control and its variations

Let $\Phi_n^{\text{BP}}(t) \in \Phi_n$ denote the phasing scheme of intersection n chosen by BP at time t . It is the phasing scheme that solves the following problem (Varaiya, 2013):

$$\Phi_n^{\text{BP}}(t) \in \arg \max_{\Phi_n \in \Phi_n} \sum_{m \in \mathcal{M}_n} w_m^{\text{BP}}(t) \bar{s}_m \phi_m(t), \quad (7)$$

where \bar{s}_m is the M-SFR of movement m during one time interval, and $w_m^{\text{BP}}(t)$ is the *weight variable* defined by

$$w_m^{\text{BP}}(t) \equiv x_m(t) - \sum_{j \in O(m)} x_j(t) r_j(t). \quad (8)$$

Obviously, BP is a distributed policy allowing intersections to make decisions independently based on neighboring information. Since the number of possible phases at any intersection tends to be small (typically four-eight), (7) can be easily solved by direct enumeration. Though simple, BP comes with robust theoretical guarantees, which say as long as the demand vector belongs to \mathcal{D}^- (the interior of \mathcal{D}), BP can ensure strong stability of the network.

Definition 3 (Strong stability). The traffic network is said to be strongly stable if (Neely, 2010, Definition 2.7):

$$\limsup_{T \rightarrow \infty} \frac{1}{T} \sum_{t=0}^{T-1} \sum_{m \in \mathcal{M}} \mathbb{E}\{x_m(t)\} < \infty. \quad (9)$$

Clearly, strong stability is stronger than rate stability, and it implies rate stability (Neely, 2010, Theorem 2.8). We refer the readers to Varaiya (2013) for the rigorous stability proof of BP.

We note that BP assumes vehicles always discharge with M-SFR once they are arranged to pass. This assumption, however, can be easily violated. That is because real-time SFR can vary dramatically due to fast-changing traffic conditions. Li and Jabari (2019, 2020) relaxed this M-SFR assumption and proposed a PWBP algorithm which assigns higher weights to vehicles closer to the intersection, and replaces the M-SFR by the actual number of passing vehicles:

$$\Phi_n^{\text{PWBP}}(t) \in \arg \max_{\Phi_n \in \Phi_n} \sum_{m \in \mathcal{M}_n} w_m^{\text{PWBP}}(t) q_i(t, \Phi_n), \quad (10)$$

with $w_m^{\text{PWBP}}(t)$ defined by

$$w_m^{\text{PWBP}}(t) \equiv \sum_{v \in V_m(t)} \frac{d(v)}{l(m)} - \sum_{j \in O(m)} \sum_{v' \in V_j(t)} \frac{l(j) - d(v')}{l(j)} r_j(t),^3 \quad (11)$$

where v or v' is a vehicle, $V_m(t)$ is all vehicles queueing in m at t (hence $|V_m(t)| = x_m(t)$), $l(m)$ is length of the link that m originates from, $d(v)$ is the distance from the most-upstream point of vehicle v 's located link to v 's current location. The motivation behind (10)-(11) is that vehicles near the intersection are more urgent and hence deserve higher weights. The rigorous stability proof of PWBP can be found in Li and Jabari (2019).

PWBP abandons the M-SFR discharging assumption, but it assumes the actual number of passing vehicles can be predicted precisely in the stability proof and does not discuss the influence of prediction accuracy on the model. Later, Wang et al. (2022) proposed another way to cope with the M-SFR assumption considering the existence of phase switching loss. They assumed that each time the signal switches the phase, it would experience a fixed switching loss during which no vehicles could pass the intersection. Vehicles can discharge (with M-SFR) only after the switching loss. They introduced a switching-curve and formulated the SCBP to prevent the signal from switching too frequently. The SCBP were then extended to policy-gradient reinforcement learning SCBP (Learned-Extended-SCBP, LESCOBP) for practical implementation⁴. With LESCOBP, each intersection can either choose a phase to maximize the pressure function or keep the phase strategy unchanged:

$$\Phi_n^{\text{LESCBP}}(t) \in \begin{cases} \arg \max_{\Phi_n \in \Phi_n} \sum_{m \in \mathcal{M}_n} w_m^{\text{LESCBP}}(t) \bar{s}_m \phi_m(t), & \text{if } \psi_n(t) > 0 \\ \Phi_n^{\text{LESCBP}}(t-1), & \text{if } \psi_n(t) \leq 0 \end{cases}, \quad (12)$$

where $w_m^{\text{LESCBP}}(t)$ is the weight coefficient with a slight difference from $w_m^{\text{PWBP}}(t)$ in the position weights for stopped and moving vehicles, and $\psi_n(t)$ is the phase-switch indicator calculated by

$$\psi_n(t) = \max_{\Phi_n \in \Phi_n} \sum_{m \in \mathcal{M}_n} w_m^{\text{LESCBP}}(t) \bar{s}_m \phi_m(t) - \left(\sum_{m \in \mathcal{M}_n} w_m^{\text{LESCBP}}(t) \bar{s}_m \phi_m(t-1) + \alpha \|\mathbf{x}_n(t)\|^\beta \right), \quad (13)$$

where $\alpha \|\mathbf{x}_n(t)\|^\beta$ is the switching-curve function, α and β are positive constants that need to be learned (using reinforcement learning) and calibrated, and $\|\mathbf{x}_n(t)\|$ is 1-norm of the column vector

³There are two versions of PWBP. One uses absolute value (Li and Jabari, 2019) when calculating $w_m^{\text{PWBP}}(t)$, and the other does not (Li and Jabari, 2020). Both of them can guarantee network stability. Here we use the one that does not have absolute value.

⁴Backpressure is also called max pressure in some literature. For example, LESCOBP is named as LESCMP (Learned-Extended-Switching-Curve based Max Pressure) in Wang et al. (2022). This paper uses the name of BP uniformly for the sake of clarity.

that equals the summation of all the queue lengths of intersection n . With the switching rule given by (12), the switching frequency will decrease with an increase in traffic demand, since a higher traffic demand usually leads to longer queue lengths, making the switching condition harder to be satisfied.

There also exist many other variations of BP (Gregoire et al., 2014b; Rey and Levin, 2019; Levin et al., 2020; Mercader et al., 2020; Li et al., 2021; Xu et al., 2022). Their common point is that they all assumed either a fixed M-SFR or a completely known I-SFR. However, no efforts have been made to investigate whether the ADR is changed when using M-SFR or I-SFR. In addition, the BP-based models' performances (e.g., stability, delay) with only partial knowledge of I-SFR still needs to be discovered. In the next section, we will answer how ADR changes with the knowledge level of I-SFR. Following that, we will formulate BP with predicted I-SFR and demonstrate its performance.

3. Changes in ADR

3.1. I-SFR and M-SFR

The U.S. Highway Capacity Manual (HCM) (Transportation Research Board, 2010) defines SFR as the maximum flow rate in lane groups per hour when the traffic signal always displays green. SFR can be obtained by 3600 s dividing the mean saturation headway. The value of SFR can be influenced by many factors such as vehicle compositions (e.g., percentage of buses, heavy vehicles), interference from parking vehicles, non-motorized vehicles, and pedestrians (Milazzo et al., 1998; Allen et al., 1998; Lin et al., 2016). In field investigation of a fixed movement, the observed SFR can vary a lot because of the continuously changing traffic conditions. Such variations could be significant even when the observation intervals are short. Conventional traffic controllers usually use M-SFR for signal timing (He and Hou, 2012) and efficiency indices (e.g., capacity, delay, waiting time, queue length) calculation (Hurdle, 1984). Limited by the technology, conventional controllers are hard to know I-SFR and usually ignore it. Although the distribution of I-SFR can be easily obtained through field investigations, an accurate prediction of I-SFR in real time is usually difficult and seems useless in traditional (fixed-time) control. However, with the popularity of video cameras and the rapid development of connected vehicle technology, it becomes possible and even convenient for the controller to monitor traffic conditions in real time. Furthermore, if we know I-SFR in real-time traffic control, we could better match the supply and demand at intersections. Therefore, it is valuable to theoretically analyze the influence of I-SFR on traffic control.

An I-SFR can be regarded as a random event whose outcome is influenced by real-time traffic conditions. For each movement m , the set of all its possible I-SFR events is denoted by S_m . For a movement group \mathcal{M} , we can express the set of all its possible joint I-SFR events (denoted by E) by $E = \times_{m \in \mathcal{M}} S_m$. Without online observation of traffic conditions, we can "guess" each event's probability from the historical data of movement m . Suppose the I-SFRs of all movements are independent⁵, the probability of any joint event can be easily obtained by timing the probability of all related events together. Taking $|E|$ as the total number of all possible joint events in E , we can calculate m 's M-SFR by

$$\bar{s}_m = \mathbb{E}\{s_m\} = \sum_{e=1}^{|E|} p^e s_m^e, \quad (14)$$

where s_m^e is m 's I-SFR in the e th joint event, and p^e is the probability of the e th joint event of E with $\sum_{e=1}^{|E|} p^e = 1$.

⁵Although this assumption is a bit strict, our observations from the field data show that it is generally reasonable. More discussions about this assumption can be found in Appendix 2.

3.2. \mathcal{D}_0 : ADR with knowledge of M-SFR

When the controller only knows M-SFR, the capacity of a movement can be obtained by timing its M-SFR and (effective) green ratio (Transportation Research Board, 2010):

$$\bar{c}_m = \bar{s}_m \bar{g}_m, \quad (15)$$

where \bar{c}_m is m 's capacity considering M-SFR, and $\bar{g}_m \in [0, 1]$ is m 's average green ratio. \bar{g}_m can be calculated as the expectation of $\phi_m(t)$: $\bar{g}_m = \mathbb{E}\{\phi_m(t)\}$. Considering all movements within the network, we denote the green ratio vector as $\mathbf{g} = \begin{pmatrix} g_1 \\ \vdots \\ g_{|\mathcal{M}|} \end{pmatrix}$, which consists of all movements' green ratios. We denote a complete set of all possible \mathbf{g} as \mathcal{G} . Generally, \mathcal{G} can be formulated as a linear constraint of \mathbf{g} :

$$\mathcal{G} = \{\mathbf{g} : \mathbf{K} \cdot \mathbf{g} \leq \mathbf{h}\}, \quad (16)$$

where \mathbf{K} is a constraint matrix for all conflicting movements and 0-boundaries, and \mathbf{h} is a (column) vector with proper dimensions. For example, for a single intersection with two conflicting through movements, we have $g_1 + g_2 \leq 1$, $g_1 \geq 0$, and $g_2 \geq 0$. Hence $\mathbf{K} = \begin{pmatrix} 1 & 1 \\ -1 & 0 \\ 0 & -1 \end{pmatrix}$ and $\mathbf{h} = \begin{pmatrix} 1 \\ 0 \\ 0 \end{pmatrix}$. It is easy to verify that \mathcal{G} is a convex polyhedron region.

According to Theorem 1, to stabilize the queues, the arrival rate of movement m (denoted by $\lambda_m \geq 0$) should not exceed its capacity: $\lambda_m \leq c_m$. Therefore, the ADR only with the knowledge of M-SFR, denoted by \mathcal{D}_0 , can be expressed by $\mathcal{D}_0 = \{(\mathbf{a}, \mathbf{R}) : \mathbf{0} \leq (\mathbf{I} - \mathbf{R})^{-1} \cdot \mathbf{a} \leq \bar{\mathbf{s}} \cdot \bar{\mathbf{g}}, \bar{\mathbf{g}} \in \mathcal{G}\}$. It is easy to verify that \mathcal{D}_0 is convex because \mathcal{G} is convex, and \mathcal{D}_0 can also be expressed as

$$\mathcal{D}_0 = \{(\mathbf{a}, \mathbf{R}) : (\mathbf{I} - \mathbf{R})^{-1} \cdot \mathbf{a} = \bar{\mathbf{s}} \cdot \bar{\mathbf{g}}, \bar{\mathbf{g}} \in \mathcal{G}\}, \quad (17)$$

where $\bar{\mathbf{s}} = \begin{pmatrix} \bar{s}_1 & & \\ & \ddots & \\ & & \bar{s}_{|\mathcal{M}|} \end{pmatrix}$ is the M-SFR matrix.

3.3. \mathcal{D}_1 : ADR with full knowledge of I-SFR

When the controller has full knowledge of I-SFR, it can allocate different green ratios for different I-SFRs, hence

$$c_m = \mathbb{E}\{s_m(t)\phi_m(t)\} = \sum_{e=1}^{|E|} p^e s_m^e g_m^e, \quad (18)$$

where c_m is m 's capacity considering I-SFR, and $g_m^e \in [0, 1]$ is m 's green ratio when the e th joint event happens: $g_m^e = \mathbb{E}\{\phi_m(t)|e\}$. Clearly, \bar{c}_m and c_m are the same only when $s_m(t)$ and $\phi_m(t)$ are independent. We note that in traditional traffic scenarios, $s_m(t)$ and $\phi_m(t)$ are usually independent. That is because the controller can hardly observe or estimate I-SFR with traditional technology. Hence it cannot adjust the green ratio according to I-SFR.

Similarly, the ADR with full knowledge of I-SFR, denoted by \mathcal{D}_1 , can be expressed by $\mathcal{D}_1 = \{(\mathbf{a}, \mathbf{R}) : \mathbf{0} \leq (\mathbf{I} - \mathbf{R})^{-1} \cdot \mathbf{a} \leq \sum_{e=1}^{|E|} p^e \cdot \mathbf{s}^e \cdot \mathbf{g}^e, \mathbf{g}^e \in \mathcal{G}\}$. Similar to \mathcal{D}_0 , \mathcal{D}_1 is convex and can also be expressed as

$$\mathcal{D}_1 = \{(\mathbf{a}, \mathbf{R}) : (\mathbf{I} - \mathbf{R})^{-1} \cdot \mathbf{a} = \sum_{e=1}^{|E|} p^e \cdot \mathbf{s}^e \cdot \mathbf{g}^e, \mathbf{g}^e \in \mathcal{G}\}, \quad (19)$$

where $\mathbf{s}^e = \begin{pmatrix} s_1^e & & \\ & \ddots & \\ & & s_{|\mathcal{M}|}^e \end{pmatrix}$ is the I-SFR matrix under the e th joint event.

Example 1. We show the difference between \mathcal{D}_0 and \mathcal{D}_1 through a single intersection with only two conflicting through movements (hence \mathbf{R} is a zero matrix). Suppose for each time interval, movement 1 has two possible I-SFR values, 1 and 2 (veh/time-interval) with a probability of 0.3 and 0.7, respectively; movement 2 has two possible I-SFR values, 1 and 2 with a probability of 0.5 and 0.5, respectively. Obviously, $|E| = 4$. We let $(s_1^1, s_1^2, s_1^3, s_1^4) = (1, 2, 1, 2)$ and $(s_2^1, s_2^2, s_2^3, s_2^4) = (1, 1, 2, 2)$, hence $(p^1, p^2, p^3, p^4) = (0.15, 0.35, 0.15, 0.35)$. The M-SFR matrix $\bar{s} = \sum_{e=1}^4 p^e \begin{pmatrix} s_1^e \\ s_2^e \end{pmatrix} = \begin{pmatrix} \bar{s}_1 \\ \bar{s}_2 \end{pmatrix} = \begin{pmatrix} 1.7 \\ 1.5 \end{pmatrix}$. We show \mathcal{D}_0 and \mathcal{D}_1 in Fig. 4 based on (17) and (19). It is clear that, $\mathcal{D}_0 \subset \mathcal{D}_1$, and \mathcal{D}_1 has a larger upper bound (frontier) and hence a larger size (increased by 19.9%) compared with \mathcal{D}_0 . Note that, with full knowledge of I-SFR, if we always assign green to movement 1 when movement 1's I-SFR is 2, and assign green to movement 2 when movement 1's I-SFR is 1, that is, we let $(g^1, g^2, g^3, g^4) = \begin{pmatrix} 0 & 1 & 0 & 1 \\ 1 & 0 & 1 & 0 \end{pmatrix}$, then capacity $c = \begin{pmatrix} 0.7*2 \\ 0.15*1+0.15*2 \end{pmatrix} = \begin{pmatrix} 1.4 \\ 0.45 \end{pmatrix}$; if we always assign green to movement 2 when movement 2's I-SFR is 2, and assign green to movement 1 when movement 2's I-SFR is 1, that is, we let $(g^1, g^2, g^3, g^4) = \begin{pmatrix} 1 & 1 & 0 & 0 \\ 0 & 0 & 1 & 1 \end{pmatrix}$, then capacity $c = \begin{pmatrix} 0.15*1+0.35*2 \\ 0.5*2 \end{pmatrix} = \begin{pmatrix} 0.85 \\ 1 \end{pmatrix}$.

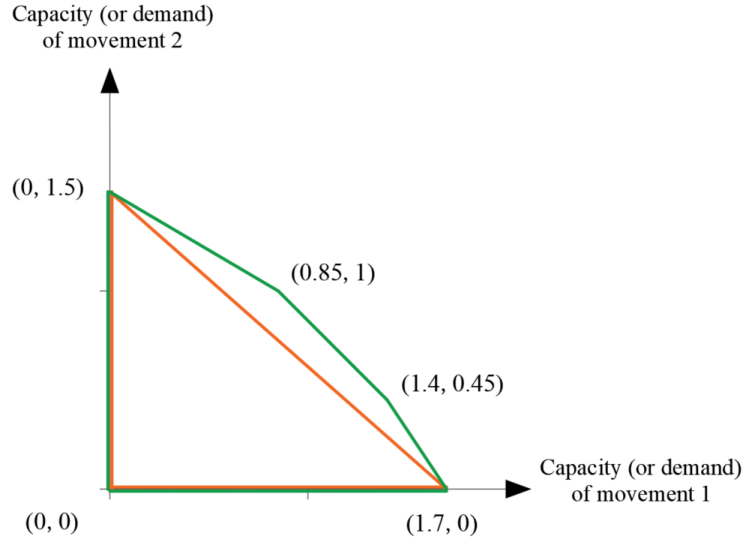


Fig. 4: ADRs in Example 1, \mathcal{D}_0 's hull: orange, \mathcal{D}_1 's hull: green.

In this simple example, we can easily find that the ADR with full knowledge of I-SFR (\mathcal{D}_1) has a larger upper bound than the ADR with only knowledge of M-SFR (\mathcal{D}_0). We will now prove this strictly.

Theorem 2. \mathcal{D}_1 contains \mathcal{D}_0 and has a larger upper bound than \mathcal{D}_0 .

Proof. We shall prove this theorem through two steps: 1) prove $\mathcal{D}_0 \subset \mathcal{D}_1$, 2) prove the upper bound of \mathcal{D}_1 is larger than the upper bound of \mathcal{D}_0 .

Step 1. Because \mathcal{G} is a convex polyhedron region, from the definition of the convex set, we can always find $|E|$ number of $g^e \in \mathcal{G}$ to express \bar{g} with

$$\bar{g} = \sum_{e=1}^{|E|} p^e \cdot g^e. \quad (20)$$

Recall that p^e is the joint event probability with $\sum_e p^e = 1$. For any $\bar{g} \in \mathcal{G}$, we can let $g^1 = \dots = g^{|E|} = \bar{g}$ satisfy (20), then $\sum_{e=1}^{|E|} p^e \cdot s^e \cdot g^e = (\sum_{e=1}^{|E|} p^e \cdot s^e) \cdot \bar{g} = \bar{s} \cdot \bar{g}$. In this case, the control policy

with full knowledge of I-SFR is the same as the control policy with only knowledge of M-SFR. Hence, $\mathcal{D}_0 \subset \mathcal{D}_1$.

Step 2. We first choose a \bar{g} such that $\bar{s} \cdot \bar{g}$ is at the upper bound of \mathcal{D}_0 . Obviously, \bar{g} must be at the upper bound of \mathcal{G} . We let $\mathbf{g}^1 = \dots = \mathbf{g}^{|E|} = \bar{g}$, hence $\sum_{e=1}^{|E|} p^e \cdot \mathbf{s}^e \cdot \mathbf{g}^e = \bar{s} \cdot \bar{g}$. We then choose a group of collaborative movements $\{m_1, m_2, \dots\}$ that can be discharged simultaneously in one interval, and choose another group of collaborative movements $\{\mu_1, \mu_2, \dots\}$ so that $\{m_1, m_2, \dots\}$ and $\{\mu_1, \mu_2, \dots\}$ are conflicting. Denoting Δg as a small positive value, we choose a joint event e_1 and add $\frac{\Delta g}{p^{e_1}}$ to $g_{m_1}^{e_1}, g_{m_2}^{e_1}, \dots$ (the green ratio of movements $\{m_1, m_2, \dots\}$ in joint event e_1). Because of the constraint of conflicting movements, we need to subtract $\frac{\Delta g}{p^{e_1}}$ from $g_{\mu_1}^{e_1}, g_{\mu_2}^{e_1}, \dots$. On the other hand, we choose another joint event e_2 and add $\frac{\Delta g}{p^{e_2}}$ to $g_{\mu_1}^{e_2}, g_{\mu_2}^{e_2}, \dots$. Similarly, we need to subtract $\frac{\Delta g}{p^{e_2}}$ from $g_{m_1}^{e_2}, g_{m_2}^{e_2}, \dots$. The chosen e_1 and e_2 satisfy some conditions, as shown below:

$$\begin{array}{cc} \text{joint event } e_1: & \text{joint event } e_2: \end{array}$$

$$\dots \begin{pmatrix} \vdots \\ g_{m_1}^{e_1} \\ g_{m_2}^{e_1} \\ \vdots \\ g_{\mu_1}^{e_1} \\ g_{\mu_2}^{e_1} \\ \vdots \end{pmatrix} \begin{array}{l} + \frac{\Delta g}{p^{e_1}} \\ + \frac{\Delta g}{p^{e_1}} \\ \\ - \frac{\Delta g}{p^{e_1}} \\ - \frac{\Delta g}{p^{e_1}} \\ \\ \end{array} \dots \begin{pmatrix} \vdots \\ g_{m_1}^{e_2} \\ g_{m_2}^{e_2} \\ \vdots \\ g_{\mu_1}^{e_2} \\ g_{\mu_2}^{e_2} \\ \vdots \end{pmatrix} \begin{array}{l} - \frac{\Delta g}{p^{e_2}} \\ - \frac{\Delta g}{p^{e_2}} \\ \\ + \frac{\Delta g}{p^{e_2}} \\ + \frac{\Delta g}{p^{e_2}} \\ \\ \end{array} \dots, \text{ where the chosen } e_1 \text{ and } e_2 \text{ satisfy: } \begin{cases} s_{m_1}^{e_1} > s_{m_1}^{e_2} \\ s_{m_2}^{e_1} > s_{m_2}^{e_2} \\ \vdots \\ s_{\mu_1}^{e_1} < s_{\mu_1}^{e_2} \\ s_{\mu_2}^{e_1} < s_{\mu_2}^{e_2} \\ \vdots \end{cases}.$$

Because I-SFRs of different movements are independent, we can always find two joint events that satisfy the above inequality group. After the above modifications to green ratios of e_1 and e_2 , we can calculate the new movement capacity for any $m \in \{m_1, m_2, \dots\} \cup \{\mu_1, \mu_2, \dots\}$ as:

$$\begin{cases} \sum_e p^e s_{m_1}^e g_{m_1}^{e, \text{new}} = \sum_e p^e s_{m_1}^e g_{m_1}^e + p^{e_1} s_{m_1}^{e_1} \frac{\Delta g}{p^{e_1}} - p^{e_2} s_{m_1}^{e_2} \frac{\Delta g}{p^{e_2}} = \sum_e p^e s_{m_1}^e g_{m_1}^e + \Delta g (s_{m_1}^{e_1} - s_{m_1}^{e_2}) > \sum_e p^e s_{m_1}^e g_{m_1}^e \\ \vdots \\ \sum_e p^e s_{\mu_1}^e g_{\mu_1}^{e, \text{new}} = \sum_e p^e s_{\mu_1}^e g_{\mu_1}^e - p^{e_1} s_{\mu_1}^{e_1} \frac{\Delta g}{p^{e_1}} + p^{e_2} s_{\mu_1}^{e_2} \frac{\Delta g}{p^{e_2}} = \sum_e p^e s_{\mu_1}^e g_{\mu_1}^e + \Delta g (s_{\mu_1}^{e_2} - s_{\mu_1}^{e_1}) > \sum_e p^e s_{\mu_1}^e g_{\mu_1}^e \\ \vdots \end{cases}.$$

As we can see, the capacity of each movement $m \in \{m_1, m_2, \dots\} \cup \{\mu_1, \mu_2, \dots\}$ is further increased as a result of the modifications. This means a capacity vector beyond the upper bound of \mathcal{D}_0 is achieved by adjusting the green ratios in different joint events with the help of I-SFR information, implying that the upper bound of \mathcal{D}_1 is larger than the upper bound of \mathcal{D}_0 . We notice that as long as the chosen initial point \bar{g} satisfies that $\bar{g}_{m_1}, \bar{g}_{m_2}, \dots, \bar{g}_{\mu_1}, \bar{g}_{\mu_2}, \dots \neq 0$ or 1, there always exist a $\Delta g > 0$ to realize the improvements in upper bound. This completes the proof. \square

We further show an example for Step 2 in the proof.

Example 2. Continue with the settings in Example 1. We choose an initial upper bound point of \mathcal{D}_0 with $\mathbf{g}^e = \bar{\mathbf{g}} = \begin{pmatrix} 0.7 \\ 0.3 \end{pmatrix}$, and the corresponding capacity vector $\mathbf{c} = \begin{pmatrix} 0.7*1.7 \\ 0.3*1.5 \end{pmatrix} = \begin{pmatrix} 1.19 \\ 0.45 \end{pmatrix}$. Take movement 1 as m_1 and movement 2 as μ_1 in the proof, and take joint event 2 as e_1 and joint event 3 as e_2 . Moreover, we set $\Delta g = 0.105$. After the modifications to \mathbf{g}^2 and \mathbf{g}^3 , we have $(\mathbf{g}^1, \mathbf{g}^{2, \text{new}}, \mathbf{g}^{3, \text{new}}, \mathbf{g}^4) = \begin{pmatrix} 0.7 & 1 & 0 & 0.7 \\ 0.3 & 0 & 1 & 0.3 \end{pmatrix}$. The new capacity vector $\mathbf{c}^{\text{new}} = \begin{pmatrix} 0.15*1*0.7+0.35*2*1+0+0.35*2*0.7 \\ 0.15*1*0.3+0+0.15*2*1+0.35*2*0.3 \end{pmatrix} = \begin{pmatrix} 1.295 \\ 0.555 \end{pmatrix} > \mathbf{c}$. Fig. 5 shows that \mathbf{c}^{new} moves to \mathcal{D}_1 's upper bound coincidentally.

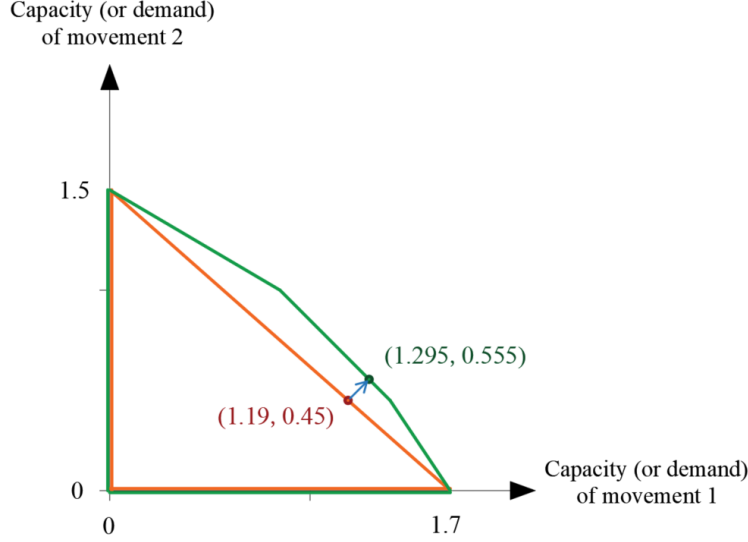


Fig. 5: Change from c to c^{new} in Example 2.

In general, [Theorem 2](#) implies that if a technology can help the controller obtain full knowledge of I-SFR, the ADR of the network can be enlarged compared with only using the knowledge of M-SFR.

3.4. \mathcal{D}_θ : ADR with partial knowledge of I-SFR

Even with advanced technology, such as connected vehicles and machine learning techniques, it is still hard to acquire full knowledge of I-SFR. Usually, the I-SFR can only be successfully predicted with a certain probability. We suppose the controller can predict the I-SFR with a *success rate* of θ . With a probability of $1 - \theta$, the controller fails to predict, and the I-SFR is in a state of “unknown”. In case of an unknown I-SFR for the next time interval, the controller will randomly “guess” an I-SFR based on the historical data. A reasonable strategy is to make the guessing probability coincident with the real probability in historical data. It can be easily verified that the predicted I-SFR (denoted by $\hat{s}_m(t)$) is unbiased: if the controller succeeds in predicting, then $\hat{s}_m(t) = s_m(t)$, hence $\mathbb{E}\{\hat{s}_m(t) | \text{“succeed”}\} = \mathbb{E}\{s_m(t)\}$; otherwise, if it fails to predict, $\mathbb{E}\{\hat{s}_m(t) | \text{“fail”}\} = \sum_{e=1}^{|E|} p^e \cdot s_m^e = \bar{s}_m = \mathbb{E}\{s_m(t)\}$. Hence, $\mathbb{E}\{\hat{s}_m(t)\} = \mathbb{E}\{s_m(t)\}$.

In an extreme case with $\theta = 0$, the controller always needs to “guess”, and the capacity vector c is

$$c|_{\theta=0} = \underbrace{\sum_{e'=1}^{|E|} p^{e'} \cdot s^{e'}}_{e' \text{ happens}} \cdot \underbrace{\sum_{e=1}^{|E|} p^e \cdot g^e}_{\text{guesses it is } e} = \bar{s} \cdot \bar{g}, \quad g^e, \bar{g} \in \mathcal{G}, \quad (21)$$

which means that such a random guess when $\theta = 0$ is equivalent to the condition with only knowledge of M-SFR, hence $c_m|_{\theta=0} = \bar{c}_m$ for each movement. Suppose the success rates of prediction for different movements are independent. The capacity vector c given θ is

$$\begin{aligned} c|_\theta &= \mathbb{E}\{s(t)\phi(t|\theta)\} = \sum_{e'=1}^{|E|} p^{e'} \cdot s^{e'} \cdot [\theta \cdot g^{e'} + (1 - \theta) \cdot \sum_{e=1}^{|E|} p^e \cdot g^e] \\ &= \theta \cdot \sum_{e=1}^{|E|} p^e \cdot s^e \cdot g^e + (1 - \theta) \cdot \bar{s} \cdot \sum_{e=1}^{|E|} p^e \cdot g^e, \quad g^e \in \mathcal{G}, \quad (22) \end{aligned}$$

where $\phi(t) = \begin{pmatrix} \phi_1(t) \\ \vdots \\ \phi_{|\mathcal{M}|}(t) \end{pmatrix}$. Note that the implementation of any control strategy is limited by the level of prediction technique (represented by θ). In the remaining of this paper, we express the control strategy $\phi(t|\theta)$ by $\phi(t)$ for simplification.

When the controller can predict the I-SFR with a success rate of θ , the corresponding ADR of the network, denoted by \mathcal{D}_θ , can be expressed by

$$\mathcal{D}_\theta = \{(\mathbf{a}, \mathbf{R}) : (\mathbf{I} - \mathbf{R})^{-1} \mathbf{a} = \theta \cdot \sum_{e=1}^{|E|} p^e \cdot \mathbf{s}^e \cdot \mathbf{g}^e + (1 - \theta) \cdot \bar{\mathbf{s}} \cdot \sum_{e=1}^{|E|} p^e \cdot \mathbf{g}^e, \mathbf{g}^e \in \mathcal{G} | \theta \in [0, 1]\}. \quad (23)$$

Example 3. Continued with the settings in Example 1 (and Fig. 4), Fig. 6 additionally shows the ADR when $\theta = 0.5$. It is clear that, the upper bound of \mathcal{D}_θ is between the upper bound of \mathcal{D}_0 and \mathcal{D}_1 , and its size is increased by 11.2% compared with \mathcal{D}_0 .

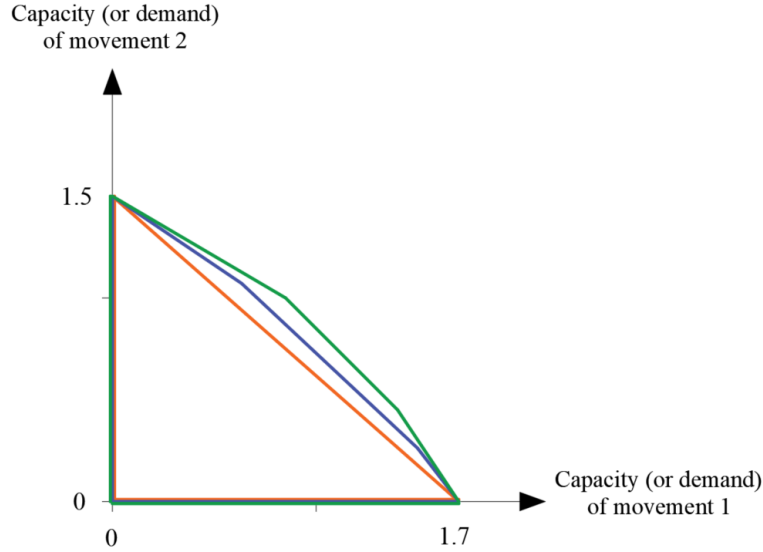


Fig. 6: ADR \mathcal{D}_θ 's hull with $\theta = 0$: orange, $\theta = 0.5$: blue, and $\theta = 1$: green.

Corollary 1. An increase in θ will enlarge the upper bound of \mathcal{D}_θ .

Proof. Based on Theorem 2, we can always find a green ratio strategy with knowledge of I-SFR to let $\sum_{e=1}^{|E|} p^e \cdot \mathbf{s}^e \cdot \mathbf{g}^e \geq \bar{\mathbf{s}} \cdot \bar{\mathbf{g}}$ be true, and there always exists $\sum_{e=1}^{|E|} p_m^e s_m^e g_m^e - \bar{s} \cdot \bar{g} > 0$ when $\bar{\mathbf{g}}$ is not at a vertex of \mathcal{G} . Therefore, given two success rates θ_a and θ_b with $\forall 0 \leq \theta_a < \theta_b \leq 1$, we can always find a green ratio strategy with knowledge of I-SFR to let $\mathbf{c}|_{\theta_b} - \mathbf{c}|_{\theta_a} = (\theta_b - \theta_a) (\sum_{e=1}^{|E|} p^e \cdot \mathbf{s}^e \cdot \mathbf{g}^e - \bar{\mathbf{s}} \cdot \bar{\mathbf{g}}) \geq \mathbf{0}$ be true, where " $>$ " holds true for some movements. Hence, \mathcal{D}_{θ_b} has a larger upper bound than \mathcal{D}_{θ_a} . This completes the proof. \square

One may note that the use of success rate θ assumes that the controller can forecast whether its prediction about I-SFR will be successful or not. In practice, whether a prediction is successful can only be known when the real I-SFR is realized. And after enough statistics, we can estimate the overall accuracy rate of the prediction, i.e., the probability that a prediction will be accurate. We shall now analyze the relationship between success rate and accuracy rate. For a movement m , suppose it has $y = |\mathcal{S}_m|$ kinds of I-SFR events with a probability of $\rho_m^1, \rho_m^2, \dots, \rho_m^y$, respectively.

Clearly, $\sum_{i=1}^y \rho_m^i = 1$. Given a success rate of θ , m 's I-SFR prediction accuracy, denoted by η , can be calculated as:

$$\eta|_{\theta} = f(\theta) = \theta + (1 - \theta) \sum_{i=1}^y (\rho_m^i)^2. \quad (24)$$

Because $\theta \in [0, 1]$ and $\sum_{i=1}^y (\rho_m^i)^2 < 1$ (when $y \geq 2$), we have that η increases monotonically with θ , and vice versa. Therefore, improving the prediction accuracy rate can help improve the success rate and hence enlarge the upper bound of ADR.

4. Network control with predicted I-SFR and network stability

4.1. S-only algorithm with predicted I-SFR

Neely designed a S-only algorithm in (Neely et al., 2005; Neely, 2010) to maximize the reserve demand (denoted by ϵ) of a communication network. The S-only algorithm makes scheduling decisions based only on the observed channel state (and hence independent of packet queue backlog). It can stabilize the queueing networks whenever the demands are inside the ADR. In a traffic network, the S-only algorithm makes phase decisions based only on the SFR (and hence independent of vehicle queue length). The objective is to maximize ϵ , with constraints to ensure that the demand is within the ADR. Based on (23), when the controller can predict I-SFR with a success rate of θ , the S-only algorithm for traffic network can be formulated as follows:

$$\text{Max:} \quad \epsilon \quad (25)$$

$$\text{s.t.:} \quad (\mathbf{I} - \mathbf{R})^{-1} \cdot (\mathbf{a} + \epsilon) \leq \theta \cdot \sum_{e=1}^{|E|} p^e \cdot \mathbf{s}^e \cdot \mathbf{g}^e + (1 - \theta) \cdot \bar{\mathbf{s}} \cdot \sum_{e=1}^{|E|} p^e \cdot \mathbf{g}^e, \quad (26)$$

$$\mathbf{K} \cdot \mathbf{g}^e \leq \mathbf{h}, \quad e = 1, 2, \dots, |E|. \quad (27)$$

The known parameters that appear as constants in the above linear program include the exogenous-arrival-rate vector \mathbf{a} , the turning ratio matrix \mathbf{R} , the success rate θ , the joint event probability $p^e, e = 1, 2, \dots, |E|$, the I-SFR matrix $\mathbf{s}^e, e = 1, 2, \dots, |E|$, the M-SFR matrix $\bar{\mathbf{s}}$, and the conflicting movement matrix/vector \mathbf{K}/\mathbf{h} . The unknowns that act as variables to be optimized in the above linear program include: the green ratio vector $\mathbf{g}^e, e = 1, 2, \dots, |E|$, and the reserve demand vector $\epsilon = \begin{pmatrix} \epsilon \\ \vdots \\ \epsilon \end{pmatrix}$ with $|\mathcal{M}|$ rows.

Define ϵ_{\max} as the maximum value of ϵ in the above problem. The value of ϵ_{\max} represents a measure of the distance between the demand rate vector $\boldsymbol{\lambda} = (\mathbf{I} - \mathbf{R})^{-1} \cdot \mathbf{a}$ and the boundary of the ADR (\mathcal{D}_{θ}). Let \mathcal{D}_{θ}^- denote the interior of \mathcal{D}_{θ} . If $\boldsymbol{\lambda}$ lies in \mathcal{D}_{θ}^- , then $\epsilon_{\max} > 0$; if $\boldsymbol{\lambda}$ locates at the upper bound of \mathcal{D}_{θ} , then $\epsilon_{\max} = 0$; if $\boldsymbol{\lambda}$ (non-negative) is outside of \mathcal{D}_{θ} , then $\epsilon_{\max} < 0$. Clearly, when $\epsilon_{\max} \geq 0$, there always exists a S-only phasing scheme $\Phi^{\text{S-only}}$ (and corresponding green ratios \mathbf{g}^e) that makes the network rate stable. We denote $\phi^{\text{S-only}}(t)$ as the vector of all movements' passing status when $\Phi^{\text{S-only}}$ is implemented by the controller.

Lemma 1. Assume that the demand rate lies in \mathcal{D}_{θ}^- , and assume the S-only strategy, $\Phi^{\text{S-only}}$, is adopted by the controller. Then, there exists a constant $\epsilon > 0$ such that $\mathbb{E}\{(\mathbf{I} - \mathbf{R}(t)) \cdot \mathbf{s}(t) \cdot \phi^{\text{S-only}}(t) - \mathbf{a}(t)\} \geq \epsilon$.

Proof. The capacity vector under the S-only strategy is $\mathbf{c}|_{\theta} = \mathbb{E}\{\mathbf{s}(t) \cdot \phi^{\text{S-only}}(t)\} = \theta \cdot \sum_{e=1}^{|E|} p^e \cdot \mathbf{s}^e \cdot \mathbf{g}^e + (1 - \theta) \cdot \bar{\mathbf{s}} \cdot \sum_{e=1}^{|E|} p^e \cdot \mathbf{g}^e$. As $\mathbb{E}\{\mathbf{R}(t)\} = \mathbf{R}$, $\mathbb{E}\{\mathbf{a}(t)\} = \mathbf{a}$, from the constraint of (26), we have $\mathbb{E}\{\mathbf{I} - \mathbf{R}(t)\} \cdot \mathbb{E}\{\mathbf{s}(t) \cdot \phi^{\text{S-only}}(t)\} - \mathbb{E}\{\mathbf{a}(t)\} \geq \epsilon$. Since $\mathbf{R}(t)$, $\mathbf{a}(t)$ and $\mathbf{s}(t) \cdot \phi^{\text{S-only}}(t)$ are

independent, and note that $\phi^{S\text{-only}}(t)$ is influenced by \mathbf{R} and is independent of $\mathbf{R}(t)$, we have $\mathbb{E}\{(\mathbf{I} - \mathbf{R}(t)) \cdot \mathbf{s}(t) \cdot \phi^{S\text{-only}}(t) - \mathbf{a}(t)\} \geq \epsilon$. When the demand rate lies in \mathcal{D}_θ^- , we have $\epsilon_{max} > 0$. Hence by setting $\epsilon = \epsilon_{max}$, we have $\mathbb{E}\{(\mathbf{I} - \mathbf{R}(t)) \cdot \mathbf{s}(t) \cdot \phi^{S\text{-only}}(t) - \mathbf{a}(t)\} \geq \epsilon_{max} > 0$. This completes the proof. \square

It is worth mentioning that although the S-only algorithm in this paper assumes \mathbf{a} , \mathbf{R} , and SFRs are known as constant parameters, they can actually be changed by traffic policies in the real world. For example, traffic demand management policy such as congestion pricing could affect \mathbf{a} a lot, map navigation could significantly influence \mathbf{R} , and automated vehicle technology may increase SFRs. These, however, are all beyond the scope of this paper. As stated in Definition 2, the ADR must be defined under a given technique background. This paper focuses on investigating how the knowledge of I-SFR would influence ADR. Hence to simplify the problem, the "given technique background" assumes \mathbf{a} , \mathbf{R} , and SFRs are all constants, and the control policy only influences green ratios. We shall now show through an example how θ would influence ϵ_{max} , given constant \mathbf{a} , \mathbf{R} and SFRs.

Example 4. Consider a simple network with only two nodes (intersections) and eight movements as shown in Fig. 7. The exogenous-arrival-rate vector $\mathbf{a} = (2, 1, 0, 0, 1.6, 1, 0, 0)^T$, and the turning ratio vector for movements $\{1, 2, \dots, 8\}$ is $(r_1, r_2, \dots, r_8) = (0.67, 0.33, 0.25, 0.27, 0.62, 0.38, 0.2, 0.8)$.

Considering the network structure, the turning ratio matrix can be written as $\mathbf{R} = \begin{pmatrix} 0 & 0 & 0 & 0 & 0 & 0 & 0 & 0 \\ 0 & 0 & 0 & 0 & 0 & 0 & 0 & 0 \\ 0 & 0 & 0 & 0 & r_3 & 0 & r_3 & 0 \\ 0 & 0 & 0 & 0 & r_4 & 0 & r_4 & 0 \\ 0 & 0 & 0 & 0 & 0 & 0 & 0 & 0 \\ 0 & 0 & 0 & 0 & 0 & 0 & 0 & 0 \\ r_7 & 0 & r_7 & 0 & 0 & 0 & 0 & 0 \\ r_8 & 0 & r_8 & 0 & 0 & 0 & 0 & 0 \end{pmatrix}$.

Assume the controller makes decisions every 10 s, and for every movement m , we suppose its I-SFR every 10 s can be 3 or 4 (veh/10 s) with an equal probability of 0.5.

Each node has three possible phases, excluding movement groups with merging conflicts, as shown in Fig. 7. We have $g_1^e + g_3^e \leq 1$, $g_1^e + g_4^e \leq 1$, $g_2^e + g_4^e \leq 1$ for Node 1, and $g_5^e + g_7^e \leq 1$, $g_5^e + g_8^e \leq 1$, $g_6^e + g_8^e \leq 1$ for Node 2. The conflicting matrix $\mathbf{K} = \begin{pmatrix} \mathbf{K}' \\ -\mathbf{I} \end{pmatrix}$, where $\mathbf{K}' = \begin{pmatrix} 1 & 0 & 1 & 0 & 0 & 0 & 0 & 0 \\ 1 & 0 & 0 & 1 & 0 & 0 & 0 & 0 \\ 0 & 1 & 0 & 1 & 0 & 0 & 0 & 0 \\ 0 & 0 & 0 & 0 & 1 & 0 & 1 & 0 \\ 0 & 0 & 0 & 0 & 1 & 0 & 0 & 1 \\ 0 & 0 & 0 & 0 & 0 & 1 & 0 & 1 \end{pmatrix}$, and the conflicting vector is $\mathbf{h} = (1, 1, 1, 1, 1, 1, 0, 0, 0, 0, 0, 0)^T$.

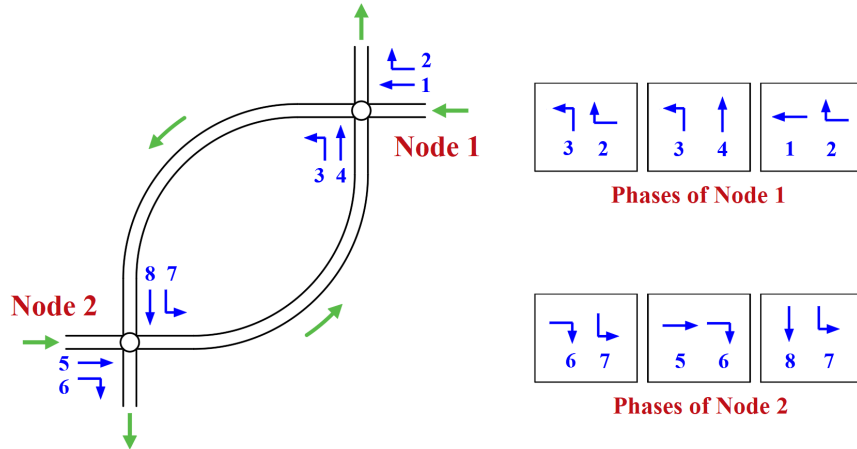


Fig. 7: Structure of a simple network and its possible phases in Example 4.

When θ takes different values from 0 to 1, ϵ_{max} of this network will also be different. We draw ϵ_{max} with different θ values in Fig. 8. Obviously, ϵ_{max} increases linearly with θ , and it equals

to 0 when $\theta = 0.485$. Since the network can only be stabilized when $\epsilon_{\max} \geq 0$, we have that the network can be rate table only when $\theta \geq 0.485$. When $\theta < 0.485$, no control algorithm can stabilize the network.

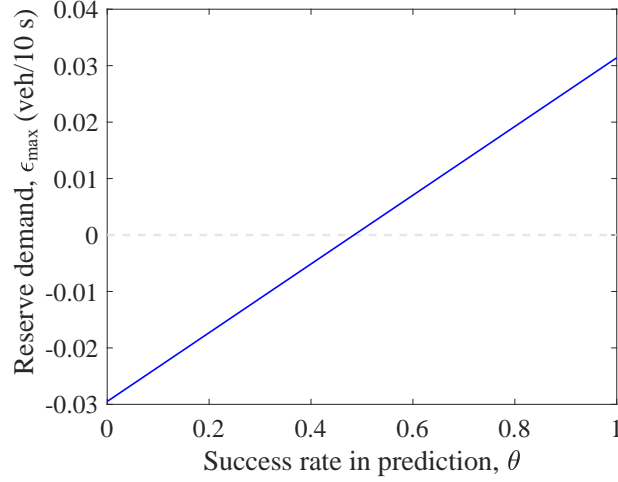


Fig. 8: Changes of ϵ_{\max} with different θ in Example 4.

4.2. Backpressure control with predicted I-SFR and its stability

When the controller can predict the I-SFR to some degree with a prediction accuracy of η , the corresponding success rate is $\theta = f^{-1}(\eta)$. We propose a BP control with predicted I-SFR, which chooses the phasing scheme that solves the following problem:

$$\Phi_n^{\text{BP},\theta}(t) \in \arg \max_{\Phi_n \in \Phi_n} \sum_{m \in \mathcal{M}_n} w_m^{\text{BP}}(t) \hat{s}_m(t) \phi_m(t). \quad (28)$$

We shall prove that the BP control with predicted I-SFR can achieve strong stability as long as the demand rate lies in \mathcal{D}_θ^- .

We define the network-wide Lyapunov functional (L) as

$$L(\mathbf{X}(t)) \equiv \frac{1}{2} \sum_{m \in \mathcal{M}} x_m^2(t), \quad (29)$$

and define the Lyapunov drift (Δ) as

$$\Delta(\mathbf{X}(t)) \equiv \mathbb{E}\{L(\mathbf{X}(t+1)) - L(\mathbf{X}(t)) | \mathbf{X}(t)\}. \quad (30)$$

Lemma 2 below provides a sufficient condition for strong stability using the definition of Lyapunov functionals.

Lemma 2. *For the Lyapunov functional (29), suppose $\mathbb{E}\{L(\mathbf{X}(0))\} < \infty$. If there exist constants $0 < K < \infty$ and $0 < \epsilon < \infty$ such that*

$$\Delta(\mathbf{X}(t)) \leq K - \epsilon \sum_{m \in \mathcal{M}} x_m(t) \quad (31)$$

holds for all $t \geq 0$ and all possible $\mathbf{X}(t)$, then the traffic network is strongly stable.

Proof. We first integrate both sides of (31) over the interval $[0, T]$ and take expectation of both sides of the inequality to obtain

$$\mathbb{E} \sum_{t=0}^{T-1} \mathbb{E}\{L(\mathbf{X}(t+1)) - L(\mathbf{X}(t)) | \mathbf{X}(t)\} \leq KT - \epsilon \left(\sum_{t=0}^{T-1} \sum_{m \in \mathcal{M}} \mathbb{E}\{x_m(t)\} \right). \quad (32)$$

Using the law of iterated expectations and telescoping sums yields

$$\mathbb{E}\{L(\mathbf{X}(T-1))\} - \mathbb{E}\{L(\mathbf{X}(0))\} \leq KT - \epsilon \left(\sum_{t=0}^{T-1} \sum_{m \in \mathcal{M}} \mathbb{E}\{x_m(t)\} \right). \quad (33)$$

Rearranging terms, dividing by ϵT , and using the fact that $L(\mathbf{X}(T-1)) > 0$, we have

$$\frac{1}{T} \sum_{t=0}^{T-1} \sum_{m \in \mathcal{M}} \mathbb{E}\{x_m(t)\} < \frac{K}{\epsilon} + \frac{\mathbb{E}\{L(\mathbf{X}(0))\}}{\epsilon T}. \quad (34)$$

Since $\mathbb{E}\{L(\mathbf{X}(0))\} < \infty$, taking a lim sup yields:

$$\limsup_{T \rightarrow \infty} \frac{1}{T} \sum_{t=0}^{T-1} \sum_{m \in \mathcal{M}} \mathbb{E}\{x_m(t)\} < \frac{K}{\epsilon}. \quad (35)$$

This completes the proof. \square

Theorem 3 (Stability of BP). Assume that arrival rates lie in \mathcal{D}_θ^- , then the BP policy with predicted I-SFR (28) ensures strong stability of the traffic network.

Proof. Substituting (3) into (29), and noting that $\max[x_m(t) - s_m(t)\phi_m(t), 0] \leq x_m(t)$, $\max[x_m(t) - s_m(t)\phi_m(t), 0]^2 \leq [x_m(t) - s_m(t)\phi_m(t)]^2$, and $\min[x_m(t), s_m(t)\phi_m(t)] \leq s_m(t)\phi_m(t)$, we have:

$$\begin{aligned} L(\mathbf{X}(t+1)) &\leq \frac{1}{2} \sum_{m \in \mathcal{M}} \{ [x_m(t) - s_m(t)\phi_m(t)]^2 \\ &\quad + [a_m(t) + r_m(t) \sum_{i \in U(m)} s_i(t)\phi_i(t)]^2 + 2x_m(t)[a_m(t) + r_m(t) \sum_{i \in U(m)} s_i(t)\phi_i(t)] \}. \end{aligned} \quad (36)$$

Substituting (36) into (30) yields:

$$\begin{aligned} \Delta(\mathbf{X}(t)) &\leq \mathbb{E} \left\{ \sum_{m \in \mathcal{M}} \left\{ -x_m(t)s_m(t)\phi_m(t) + \frac{1}{2}[s_m(t)\phi_m(t)]^2 + \frac{1}{2}[a_m(t) \right. \right. \\ &\quad \left. \left. + r_m(t) \sum_{i \in U(m)} s_i(t)\phi_i(t)]^2 + x_m(t)[a_m(t) + r_m(t) \sum_{i \in U(m)} s_i(t)\phi_i(t)] \right\} | \mathbf{X}(t) \right\}. \end{aligned} \quad (37)$$

Because $[s_m(t)\phi_m(t)]^2 + [a_m(t) + r_m(t) \sum_{i \in U(m)} s_i(t)\phi_i(t)]^2 \leq \tilde{s}^2 + \max_m [\tilde{a} + \sum_{i \in U(m)} \tilde{s}]^2$ for $m \in \mathcal{M}$, where \tilde{s} is the maximum value of the I-SFR of all possible movements, and \tilde{a} is the maximum value of all possible exogenous arrival rates. Let $\tilde{K} = \tilde{s}^2 + \max_m [\tilde{a} + \sum_{i \in U(m)} \tilde{s}]^2$, the second term plus the third term on the right-hand side of (37) is then bounded by $\frac{1}{2}|\mathcal{M}|\tilde{K}$. Rearranging terms of (37) and utilizing the properties of conditional expectation, we have

$$\Delta(\mathbf{X}(t)) \leq \frac{1}{2}|\mathcal{M}|\tilde{K} - \sum_{m \in \mathcal{M}} x_m(t) \mathbb{E}\{s_m(t)\phi_m(t) - a_m(t) - r_m(t) \sum_{i \in U(m)} s_i(t)\phi_i(t) | \mathbf{X}(t)\}, \quad (38)$$

where $x_m(t)$ is moved out of the expectation since $\mathbf{X}(t)$ is given.

Note that the controller cannot directly observe $s_m(t)$, we define the error item (denoted by \mathcal{E}) as

$$\mathcal{E}_m(t) = \hat{s}_m(t) - s_m(t). \quad (39)$$

As stated above, $\hat{s}_m(t)$ is unbiased, hence we have $\mathbb{E}\{\mathcal{E}_m(t)\} = 0$ for $m \in \mathcal{M}$. Furthermore, because $s_m(t)$ could only be observed during green, we have $\mathbb{E}\{\mathcal{E}_m(t) | \phi_m(t) = 1\} = 0$. Define a control policy Φ^{\max} for each $t \geq 0$ as

$$\Phi^{\max} = \arg \max_{\Phi \in \Phi} \left(\sum_{m \in \mathcal{M}} x_m(t) \mathbb{E}\{\hat{s}_m(t)\phi_m(t) - a_m(t) - r_m(t) \sum_{i \in U(m)} \hat{s}_i(t)\phi_i(t) | \mathbf{X}(t)\} \right). \quad (40)$$

We also have for each $t \geq 0$ that

$$\begin{aligned} & \mathbb{E}\{\hat{s}_m(t)\phi_m(t) - a_m(t) - r_m(t) \sum_{i \in U(m)} \hat{s}_i(t)\phi_i(t) | \mathbf{X}(t)\} \\ &= \mathbb{E}\{s_m(t)\phi_m(t) | \mathbf{X}(t)\} + \mathbb{E}\{\mathcal{E}_m(t)\phi_m(t) | \mathbf{X}(t)\} - \mathbb{E}\{a_m(t)\} \\ & \quad - \mathbb{E}\{r_m(t) \sum_{i \in U(m)} s_i(t)\phi_i(t) | \mathbf{X}(t)\} - \sum_{i \in U(m)} \mathbb{E}\{r_m(t)\mathcal{E}_i(t)\phi_i(t) | \mathbf{X}(t)\} \end{aligned} \quad (41)$$

Note that $\phi_m(t) = 1$ or 0, we have

$$\mathbb{E}\{\mathcal{E}_m(t)\phi_m(t) | \mathbf{X}(t)\} = \mathbb{E}\{\mathcal{E}_m(t) | \mathbf{X}(t), \phi_m(t) = 1\} \mathbb{P}\{\phi_m(t) = 1\} + 0, \quad (42)$$

and

$$\mathbb{E}\{r_m(t)\mathcal{E}_i(t)\phi_i(t) | \mathbf{X}(t)\} = \mathbb{E}\{r_m(t)\mathcal{E}_i(t) | \mathbf{X}(t), \phi_i(t) = 1\} \mathbb{P}\{\phi_i(t) = 1\} + 0 \quad (43)$$

for $i \in U(m)$.

Because $\mathcal{E}_i(t)$ and $r_m(t)$ are independent⁶, and $\mathcal{E}_m(t)$ is also independent of $x_m(t)$ given $\phi_m = 1$ for any m ⁷, we have

$$\mathbb{E}\{\mathcal{E}_m(t) | \mathbf{X}(t), \phi_m(t) = 1\} = \mathbb{E}\{\mathcal{E}_m(t) | \phi_m(t) = 1\} = 0, \quad (44)$$

and

$$\mathbb{E}\{r_m(t)\mathcal{E}_i(t) | \mathbf{X}(t), \phi_i(t) = 1\} = \mathbb{E}\{r_m(t) | \mathbf{X}(t), \phi_i(t) = 1\} \mathbb{E}\{\mathcal{E}_i(t) | \phi_i(t) = 1\} = 0. \quad (45)$$

Hence, (41) is equal to

$$\mathbb{E}\{s_m(t)\phi_m(t) - a_m(t) - r_m(t) \sum_{i \in U(m)} s_i(t)\phi_i(t) | \mathbf{X}(t)\}. \quad (46)$$

By definition, we have for each $t \geq 0$ that

⁶ $r_m(t)$ is the proportion of all vehicles from m 's upstream movements $U(m)$ that will directly join movement m at time t , hence it only influences the turning ratio of m at time $t + 1$, and can hardly influence the prediction error of m 's I-SFR at time t . $r_m(t)$ is also not influenced by $\mathcal{E}_m(t)$ logically.

⁷The relationship between $\mathcal{E}_i(t)$ and $x_m(t)$ is analyzed in detail in Appendix 3. In brief, although the information of $x_m(t)$ may help improve the prediction accuracy, $\mathcal{E}_i(t)$ is independent of $x_m(t)$.

$$\begin{aligned} \sum_{m \in \mathcal{M}} x_m(t) \mathbb{E} \{ s_m(t) \phi_m^{\max}(t) - a_m(t) - r_m(t) \sum_{i \in U(m)} s_i(t) \phi_i^{\max}(t) | \mathbf{X}(t) \} \\ \geq \sum_{m \in \mathcal{M}} x_m(t) \mathbb{E} \{ s_m(t) \phi_m^*(t) - a_m(t) - r_m(t) \sum_{i \in U(m)} s_i(t) \phi_i^*(t) | \mathbf{X}(t) \}. \end{aligned} \quad (47)$$

where $\phi_m^{\max}(t)$ represent the passing status of m at time t when Φ^{\max} is implemented, and $\phi_m^*(t)$ represents the passing status of m at time t when any other particular policy Φ^* (including the S-only policy) is implemented. Setting $\Phi^* = \Phi^{\text{S-only}}$ and plugging (47) into (38), we have

$$\Delta(\mathbf{X}(t)) \leq \frac{1}{2} |\mathcal{M}| \tilde{K} - \sum_{m \in \mathcal{M}} x_m(t) \mathbb{E} \{ s_m(t) \phi_m^{\text{S-only}}(t) - a_m(t) - r_m(t) \sum_{i \in U(m)} s_i(t) \phi_i^{\text{S-only}}(t) \}, \quad (48)$$

where the left-hand-side represents the drift under Φ^{\max} , and $\mathbf{X}(t)$ is dropped from the expectation since the S-only algorithm is independent of $\mathbf{X}(t)$.

Since we assume the demand rate lies in \mathcal{D}_θ^- , we have from Lemma 1 that there exists an $\epsilon > 0$ such that

$$\sum_{m \in \mathcal{M}} x_m(t) \mathbb{E} \{ s_m(t) \phi_m^{\text{S-only}}(t) - a_m(t) - r_m(t) \sum_{i \in U(m)} s_i(t) \phi_i^{\text{S-only}}(t) \} \geq \epsilon \sum_{m \in \mathcal{M}} x_m(t) \quad (49)$$

Substituting (49) into (48), setting $K \equiv \frac{1}{2} |\mathcal{M}| \tilde{K}$, we have by appeal to Lemma 2 that Φ^{\max} is also network stabilizing.

It remains to show that solving (40) (Φ^{\max}) is equivalent to solving (28) (the BP policy with predicted I-SFR). (40) can be rewritten as

$$\Phi^{\max} = \arg \max_{\Phi \in \Phi} \left(\sum_{m \in \mathcal{M}} x_m(t) \hat{s}_m(t) \phi_m(t) - \sum_{m \in \mathcal{M}} x_m(t) r_m(t) \sum_{i \in U(m)} \hat{s}_i(t) \phi_i(t) \right). \quad (50)$$

The term corresponding to exogenous arrivals in (40) was dropped from the optimization problem since it constitutes an additive constant to the problem. We have also applied the principle of *opportunisticly maximizing an expectation* to drop the expectations in (40) from the problem. Rearranging the orders of summation, (50) becomes

$$\Phi^{\max} = \arg \max_{\Phi \in \Phi} \sum_{m \in \mathcal{M}} \hat{s}_m(t) \phi_m(t) \left[x_m(t) - \sum_{j \in O(m)} x_j(t) r_j(t) \right] \quad (51)$$

Using the definition of $w_m^{\text{BP}}(t)$, (51) becomes

$$\Phi^{\max} = \arg \max_{\Phi \in \Phi} \sum_{m \in \mathcal{M}} w_m^{\text{BP}}(t) \hat{s}_m(t) \phi_m(t) \quad (52)$$

Since intersection movements do not interact across nodes instantaneously and $\Phi_{n_1} \cap \Phi_{n_2} = \emptyset$ for any $n_1, n_2 \in \mathcal{N}$ such that $n_1 \neq n_2$, the optimization problem naturally decomposes by intersection. That is, maximizing (52) is equivalent to solving the $|\mathcal{N}|$ problems

$$\Phi_n^{\text{BP}}(t) \in \arg \max_{\Phi_n \in \Phi_n} \sum_{m \in \mathcal{M}_n} w_m^{\text{BP}}(t) \hat{s}_m(t) \phi_m(t), \quad \forall n \in \mathcal{N}. \quad (53)$$

Hence, solving (40) turns out to be the same as solving (28). This completes the proof. \square

Similar to BP, by replacing the I-SFR or M-SFR with predicted I-SFR, we can formulate the new PWBP and LESCBP with predicted I-SFR. Limited by space, we shall not provide stability proofs for them in this paper. We will, however, investigate the performances of all BP, PWBP, and LESCBP with predicted I-SFR in the experiments section.

5. Experiments

All the above examples are simple and ideal. The network structure can be complicated in the real world, and various factors can influence the I-SFR. To see how I-SFR knowledge can affect control effectiveness, we shall demonstrate the network performance with different I-SFR prediction accuracies through calibrated simulations in this section. We will investigate various BP policies, including original BP, PWBP, and LESCOBP. We use different methods for each policy to predict the I-SFR and compare the reserve demand and average delay under each method.

5.1. Simulation model

Fig. 9 shows the network used in our simulations, which is a corridor with nine intersections on Qishan Avenue, Fuzhou, Fujian, China. With the historical data collected during the evening peak hour (from 17:30 to 18:30) from Oct 24 (Monday) to 28 (Friday), 2022 using videos, we calibrate the demands (including the vehicle compositions) of both ends of the avenue and all cross-streets. In additions, for different approaches of all nine intersections, we calibrate the turning ratios of all movements. Note that each street varies greatly (from 18 veh/h/lane to 410 veh/h/lane) and the percentage of buses of each street varies from 0% to 26.7%. We also investigate the demand of non-motorized vehicles for each intersection. The network topology, including the road lengths, widths, directions, lane layouts, and bus stops along the way, are extracted from the BaiduMap with the assistance of field surveys. The field controllers along Qishan Avenue use fixed-time control with signal coordination, and the cycle time during peak hour is as long as 196s. We built the simulation model with a microscopic simulation tool, VISSIM, as shown in Fig. 10, and the grey squares represent the bus stations on roads. The field fixed-time control plan is reproduced in the simulation to serve as the benchmark. For BP-based policies, we set the time interval to 10 s, i.e., the BP controllers make phase decisions every 10 s. Using the COM interface of VISSIM, we feed the real-time collected data from VISSIM to Python and then return the optimized policy from Python to VISSIM.



Fig. 9: Simulation network topology of Qishan Avenue, Fuzhou, Fujian, China.

5.2. I-SFR prediction methods

In order to collect the I-SFR data when a movement is discharged, we only collect the samples when the queue length is greater than or equal to 7 vehs/lane (considering the time interval



Fig. 10: Simulation model.

is 10 s). Considering the different volumes of non-motorized vehicles for each movement, we collect vehicle discharging data during the first 10 s of green and calibrate each movement's corresponding start-up lost time separately. The collected throughput data is then converted to I-SFR (veh/10-s/movement) of integers to make them consistent with the samples collected during the non-initial green phase (when the previous phase is the same as the current one). Note that for the non-initial green phase, the start-up lost time is 0 s.

We adopt three kinds of methods to predict the I-SFR, as listed below:

- “mean”: always take the M-SFR as the predicted I-SFR;
- “est”: estimate the I-SFR as the weighted average of the last four historical I-SFRs;
- “nn”: learn the I-SFR using the deep neural network, with the consideration of different attributes.

We note that:

- 1) When calculate the M-SFR, for each movement, we aggregate all I-SFR samples and take the average value of all I-SFRs as the M-SFR.
- 2) When calibrating the weights for different historical I-SFRs in the “est” method, we test different weight combinations and choose [1, 2, 3, 4] as the final choice. This means the most recent I-SFR has the highest weight of 4, followed by the second closest I-SFR with a weight of 3, and so on.
- 3) When learn the I-SFR using deep neural network, we collect different attributes, as shown in Fig. 11. We divide the road into cells of equal length (the average space that a vehicle occupies when traffic is in jam density), and extract the basic information for each cell, including occupancy (1 if occupied by a vehicle, 0 otherwise), vehicle speed (0 if empty), vehicle acceleration (0 if empty), and vehicle type. Besides, we also consider the non-motorized vehicle volume, the number of merging right-turn vehicles, the lane information, the number of bus entering or leaving the bus station (if any) within the 10 s free-flow distance, the number of vehicles within the 10 s free-flow distance of downstream link, and the number of vehicles entering or leaving the access (if any) within the 10 s free-flow distance. When training the machine learning model, the input of each sample is the attribute vector, and the label is the converted I-SFR per 10 s per movement.

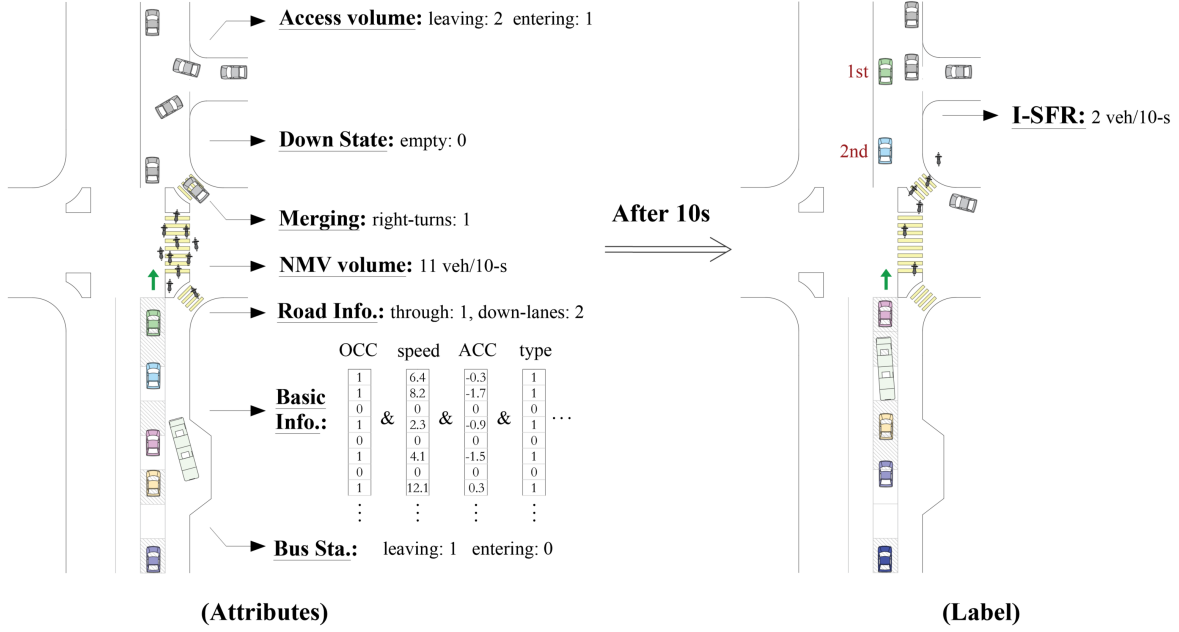


Fig. 11: Data extraction for training of the neural network model.

In order to extract I-SFR samples, we run the simulation for 10 times with different random seeds and each time lasts for 24 hours with different demand levels every 4 hours. The original BP with a predetermined M-SFR is used for generating the samples. We collect separate samples and calculate M-SFR for each movement. We also train separate learning models for each movement. We adopt the deep neural network with multi-classification as the learning model, which has one input layer, three hidden layers, and one output layer. The model is fully connected, and we pick the ReLU as its activation function in hidden layers. For the output layer, we use the softmax to activate it. The Adam optimizer is used with learning rate annealing. We use the batch normalization for each hidden layer to accelerate the training of neural network, and adopt the dropout technique for each training iteration to randomly drop neurons (with 50% probability) from the neural network to prevent over-fitting. 80% of the samples are used as the training set, and the rest 20% are used as the testing set.

Table 1 shows the prediction accuracy and prediction time of different methods. The statistical results are based on different movements. Note that although the collected real I-SFRs are integers, we allow the predicted I-SFR to be non-integers since BP does not require the SFR to be integers. When calculating accuracy, we regard the prediction to be accurate when the absolute value of error is not greater than 0.5 veh/10-s/movement. As we can see, "mean" performs the worst with a lowest average accuracy of 13.1%. With the help of more recent information, "est" improves the accuracy to 24.7%. Moreover, with a more comprehensive consideration of different real-time factors, the machine learning technique "nn" succeeds in significantly improving the average accuracy to 56.7%. Since the three methods have obvious difference in prediction accuracy, we are able to use them to test the influence of different levels of I-SFR knowledge on the network performance.

It is worth mentioning that the goal of the experiments is not to design a perfect prediction model but to validate the proposed theory. To achieve the goal, we "intentionally" develop three prediction methods with significant differences in accuracy. In addition, although a more complicated prediction method tends to have a longer computation time, all three methods cost less

than 0.01 s with an Intel i7-10875H central processing unit (CPU) with 16 cores and 16 GB memory. Hence they can all be implemented in real-time. We note that the "nn" method can compute quickly because the model is used online but trained offline. In practice, the training task can be assigned to the server. The controller only needs to update the trained model with low frequency (e.g., every hour), or the controller can train the model itself at midnight.

Table 1: Prediction accuracy of different methods.

| Method: | Prediction accuracy: | | | | | Prediction time (s): | |
|---------|----------------------|--------|-------|-------|-------|----------------------|---------|
| | average | median | SD | max | min | average | SD |
| "mean" | 0.131 | 0.131 | 0.026 | 0.182 | 0.064 | 7.0E-07 | 1.7E-07 |
| "est" | 0.247 | 0.235 | 0.057 | 0.441 | 0.179 | 3.9E-06 | 2.5E-07 |
| "nn" | 0.567 | 0.567 | 0.073 | 0.800 | 0.465 | 7.5E-03 | 4.5E-05 |

5.3. Evaluation of reserve demand

Our first experiment is to gauge the reserve demand (ϵ_{max}) of the network, given the current real traffic demand and different I-SFR prediction accuracies. A higher reserve demand implies a larger ADR boundary, hence knowing the reserve demand can help us validate the correctness of the proposed theory.

In the simulation model, when the exogenous vehicles cannot enter the link due to congestion, they will temporally stack out of link. We assume that, once the demand is beyond the ADR, the stacked vehicle number will keep increasing. Therefore, we gradually increase the exogenous demand rate of each movement, and monitor the number of stacked vehicles in real time. Once the stacked vehicle number exceeds a preset threshold, we think that the demand has reached the ADR boundary.

Specifically, by setting the initial demand to the real demand, we increase the exogenous demand rate by 5 vehs/h every 1 simulation minute. The threshold is set to 100 vehs. That is, when the total stacked vehicles' number exceeds 100 vehs, we think the corresponding real-time demand reached the ADR boundary. The increased demand (the gap between the initial demand and the real-time demand) is regarded as the reserve demand. We have more discussions about threshold choosing in Appendix 4.

We test three control policies: BP, PWBP, and LESCOBP. Each control policy uses three I-SFR prediction methods. For each combination of policy and method, we run the simulation for 30 times with different random seeds. The resulted reserve demands are demonstrated with box plots, as shown in Fig. 12 (a), (b), and (c). As we can see, for all three tested control policies, "nn" achieves the highest reserve demand, and "mean" achieves the lowest reserve demand. In other words, for any policy (of three), the reserve demand increases when the method can predict I-SFR more accurately. Take BP as an example: when the method changes from "mean" to "est" and "nn", the average reserve demand is increased by about 21% and 34%, respectively. A higher prediction accuracy can help achieve higher reserve demand because it enlarges the ADR. This experiment result is consistent with Corollary 1. We note that a more detailed inspection of the accuracy of different intersections shows that, for the critical intersection (the one that becomes congested earliest), the average accuracy of "est" is about 28%, while the average accuracy of "nn" is just 47%. This might be why the reserve demand increase from "est" to "nn" is not as noticeable as "expected".

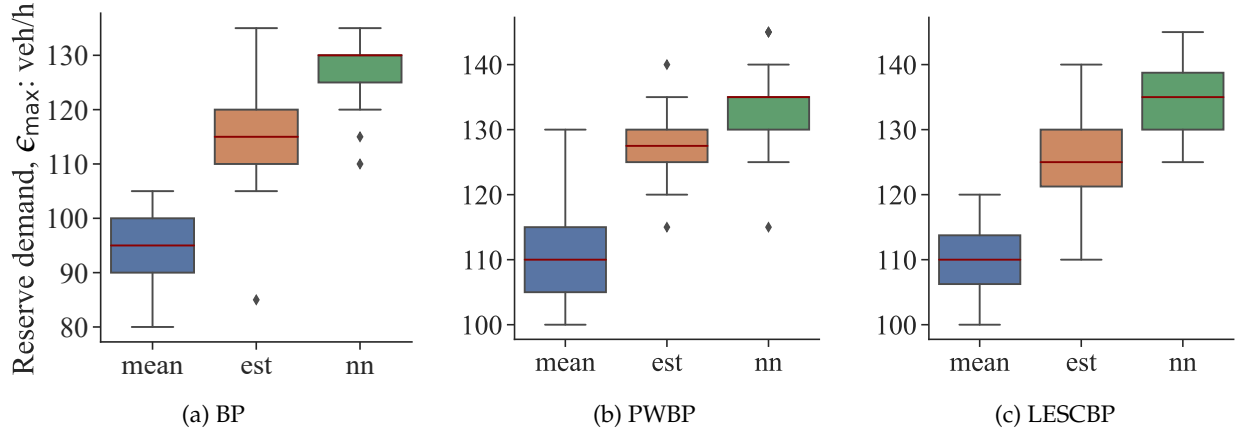


Fig. 12: Reserve demand for three control policies with different I-SFR prediction methods.

5.4. Impacts on average delay

Our second experiment aims to investigate the delay performance with different I-SFR prediction accuracies. Delay is a very important index for evaluating the performance of a traffic network. However, we only proved the queueing stability of BP with predicted I-SFR, how the delay will change with the knowledge of I-SFR is still unknown. Therefore, we want to answer this question through experiments.

Fig. 13 shows the average delay of BP with different I-SFR prediction methods when the demand is set to (a) 50% and (b) 100% levels of field demand. We note that the delay only considers motorized vehicles including cars and buses. Again, for each method, we run the simulation ten times with different random seeds, and each simulation lasts for one hour. The x-axis of Fig. 13 represents the average prediction accuracy of different movements within the network, and the y-axis represents the average delay of all vehicles per intersection. For a better comparison, we show the average delay (around 34 s) resulting from the fixed-time control in the field with a dashed line when the demand is set to the field demand. As we can see, for both demands, the mean-BP (BP using a prediction method of “mean”) has the highest delay. With a higher I-SFR prediction accuracy, est-BP reduces the delay to a much lower level. In addition, with a further improvement in prediction accuracy, nn-BP achieves the lowest delay. Obviously, more knowledge of I-SFR can effectively help BP reduce vehicle delay. Note that when the demand is half of the actual demand, the prediction accuracies of different methods are more sparse. This is because lower demand results in a smaller I-SFR sample size; hence the accuracy is less stable.

Fig. 14 (a) shows the average delay of PWBP with different I-SFR prediction methods when the demand is set to the field demand. On one hand, we can notice that PWBP performs much better than BP in general, especially when using the methods “mean” and “est”. This is consistent with the findings in Li and Jabari (2019). On the other hand, we can also see a clear tendency that the delay of PWBP decreases with an increase in I-SFR prediction accuracy. Since the delay of mean-PWBP is just slightly higher than 20 s (much lower than the fixed-time delay), we further increase the demand input by 50% to see the network performance of PWBP in more congested scenarios, as shown in Fig. 14 (b). As we can see, the delay of PWBP with different methods increases as expected, while the tendency of delay with the change of accuracy remains unchanged. Hence we can conclude that more knowledge of I-SFR can help PWBP reduce vehicle delay.

In addition, similar to Fig. 14, we show the result of LESCOBP when demand is set to 100% and

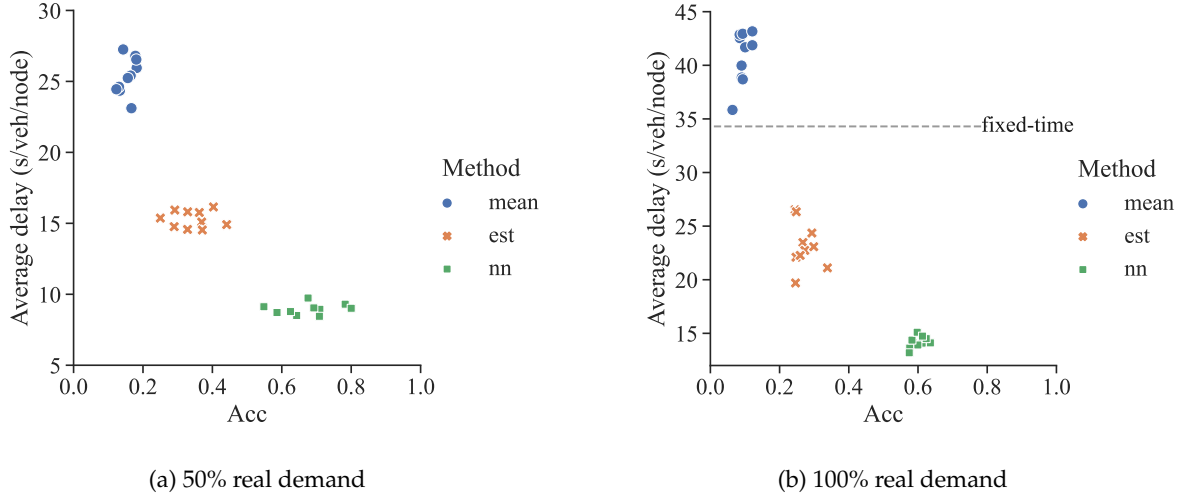


Fig. 13: Delay and accuracy for BP control.

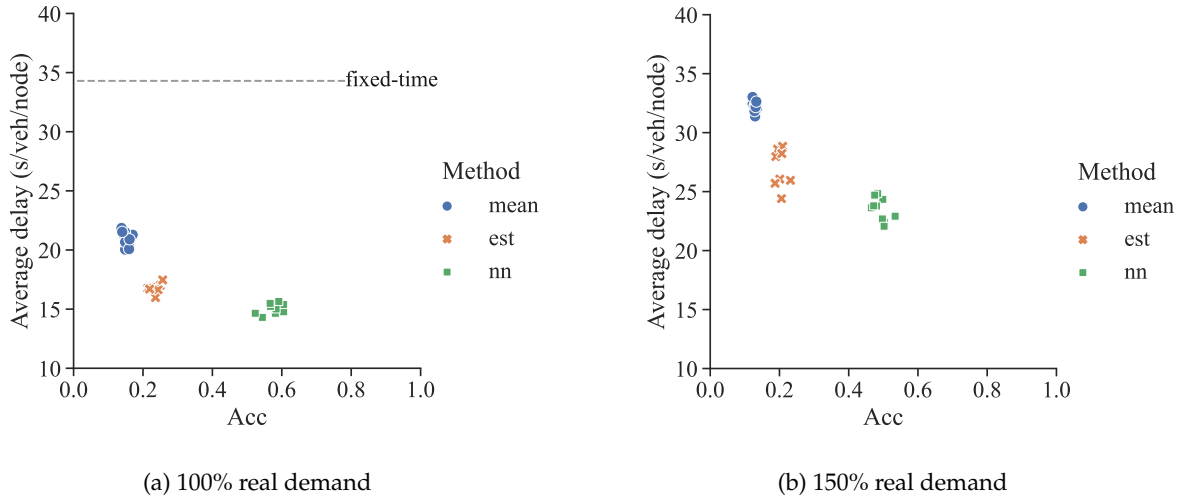


Fig. 14: Delay and accuracy for PWBP control.

150% levels of field demand in Fig. 15 (a) and (b), respectively. We can find a similar performance of LESCBP compared with PWBP and an apparent trend that the delay of LESCBP decreases with an increase in accuracy. Therefore, we conclude that more knowledge of I-SFR can help LESCBP reduce vehicle delay.

Finally, we show comparisons between “mean” and “nn” and between PWBP and LESCBP with varying demand in Fig. 16. The simulation lasts for 1.5 h. The initial demand is 50% of the field demand, which lasts for 10 min. It then increases to 100% and 150% field demand gradually. After 30 min of 150% field demand, it gradually recovers to 100% and 50% field demand. Each simulation is run ten times with different random seeds, and Fig. 16 shows the mean and standard deviation of the average vehicle delay. The solid line represents PWBP, while the dashed line represents LESCBP. Different colors represent different prediction methods. We first focus on the comparison between mean-PWBP and mean-LESCBP. Similar to the findings in Wang et al. (2022),

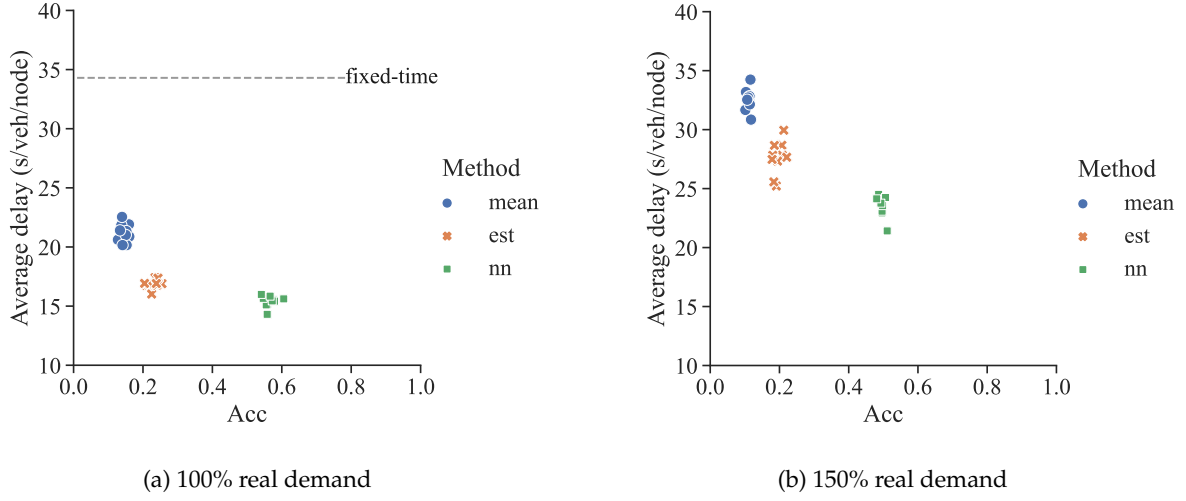


Fig. 15: Delay and accuracy for LESCBP control.

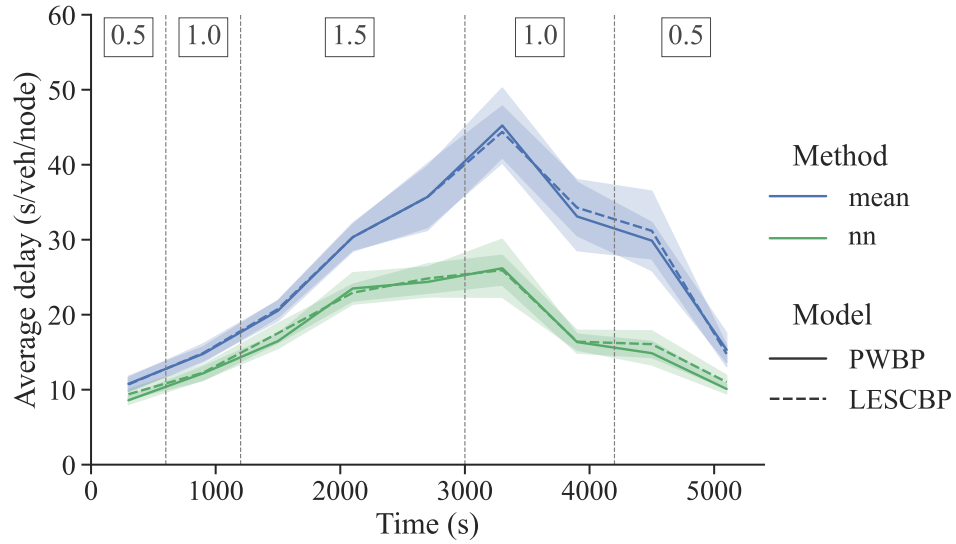


Fig. 16: Average delay under different control models and I-SFR prediction methods.

we can see that 1) when the demand is low, mean-PWBP performs slightly better than mean-LESCBP; 2) when the demand becomes high, mean-LESCBP starts to outperform mean-PWBP. These findings, which are in good agreement with the results in Wang et al. (2022), imply that we reproduced mean-LESCBP of Wang et al. (2022). We then focus on two prediction methods. Clearly, in terms of average delay, “nn” outperforms “mean” a lot during the whole period for both PWBP and LESCBP. This validates that increasing the I-SFR’s prediction accuracy helps reduce the network delay under varying demands.

6. Conclusion and outlook

The size of a network's admissible demand region (ADR) represents the network's ability to handle traffic demands. In this paper, we abandon the assumption of fixed/completely known saturation flow rate (SFR) in existing BP-based control policies and propose the controls using predicted imminent SFR (I-SFR). We analytically prove that improving the I-SFR's prediction accuracy can enlarge the size of ADR. In addition, we rigorously demonstrate that, as long as the demand rates are interior to the corresponding ADR, the BP with predicted I-SFR can guarantee network stability. Results from simulations validate the proposed theory on one hand and show the improvements in network delay with more knowledge of I-SFR on the other hand.

BP-based controls serve as the ideal tool to test the network's ADR since they can maximize the network throughput. However, this does not mean the knowledge of I-SFR only benefits BP-based control algorithms. Future research can investigate the influence of I-SFR on other real-time control policies. The key point is to realize that the traffic supply is not fixed and can be influenced by real-time traffic conditions. The three prediction methods in the simulation mainly aim to generate different levels of I-SFR. We hence did not focus on improving the prediction accuracy to the maximum degree. Although we show the advantages of the neural network prediction method over the mean I-SFR method and the heuristic method through experiments, we must point out that any prediction method has its price. A prediction method with a higher accuracy may require a more advanced hardware facility, which usually comes with greater economic investment. In the near future, when the neural network method (or other similar methods) is not feasible despite its high accuracy, it is the mean I-SFR or heuristic method that works in practice. The key is to realize that efforts to improve prediction accuracy to the extent that technology allows is worthwhile.

Appendix 1: Table of notations

See [Table 2](#).

Appendix 2: χ^2 test for independence of different movements' I-SFRs

We pick some movements that are most likely to have dependent I-SFRs and use the χ^2 test to check whether their I-SFRs are independent. All data pairs are collected simultaneously to guarantee the same surrounding environment (try our best to make their I-SFRs dependent). The results are shown in [Table 3](#). For the name of the movements, the number corresponds to the intersection number in [Fig. 9](#), "T" represents the through movement, and "L" represents the left-turn movement. In general, most movements' I-SFRs are independent when setting the significance level to $\alpha = 0.1$, and all movements are independent when setting the significance level to $\alpha = 0.01$. Hence we can conclude that, generally, it is reasonable to assume that the I-SFRs of all movements are independent. We cannot, however, 100% guarantee this assumption in the real world when the movements are from the same approach. This is also why we need the simulation experiments to verify our findings further.

Appendix 3: Relationship between prediction error and queue length

We collect 1854 saturated discharging samples and use three methods to predict the I-SFR, respectively. The prediction error (difference between the real I-SFR and the predicted one) and corresponding queue lengths are shown in [Fig. 17](#). Clearly, for all three methods, we cannot reject the assumption that "prediction error is independent of queue length".

Table 2: Notations in this paper.

| Parameter | Description |
|--|---|
| a, \tilde{a}, \mathbf{a} | exogenous arrival rate, upper bound of a , exogenous arrival rate vector |
| c, \bar{c}, \mathbf{c} | capacity with complete or partial I-SFR, capacity with M-SFR, capacity vector |
| $\mathcal{D}, \mathcal{D}^-$ | ADR (admissible demand region) with closure frontier, interior of ADR |
| $d(v)$ | distance from most-upstream point of v 's located link to v 's current location |
| \mathcal{E} | error, equal to the difference between I-SFR's real value and prediction value |
| E, E , e | set of all joint I-SFR events: $E = \times_{m \in \mathcal{M}} S_m$, size of E , an event: $e \in E$ |
| $F(\cdot), \psi$ | switching curve in LESCBP, switch function in LESCBP |
| $g, \bar{g}, \mathbf{g}, \mathcal{G}$ | (effective) green ratio, average green ratio, green ratio vector, \mathbf{g} 's complete set |
| \mathbf{h} | (column) constraint vector of signalized intersection |
| i/j | m 's upstream/downstream movement |
| K, \tilde{K} | positive constants |
| \mathbf{K} | constraint matrix for all conflicting movements and 0-boundaries |
| \mathcal{L} | set of all directed links |
| $L(\cdot), \Delta(\cdot)$ | network-wide Lyapunov function, Lyapunov drift function |
| $l(m)$ | length of the link that m originates from |
| $\mathcal{M}, \mathcal{M}_n, \mathcal{M} $ | set of all movements, set of n 's movements, number of all movements |
| m (and μ) | a movement |
| $n, \mathcal{N}, \mathcal{N} $ | a node, set of all network nodes, number of all network nodes |
| $O(m)$ | set of m 's all downstream movements |
| p^e | probability of the e th joint event |
| q_m | actual departure of m |
| r_m, \mathbf{R} | average turning ratio of movement m , average turning ratio matrix |
| S_m | set of all I-SFR events in m |
| $s, \bar{s}, \hat{s}, \tilde{s}, \mathbf{s}$ | I-SFR, M-SFR, estimated I-SFR, upper-bound of I-SFR, I-SFR vector |
| t, T | time of decision, upper bound of time |
| $U(m)$ | set of m 's all upstream movements |
| v, V_m | a vehicle, all vehicles queueing in m |
| w | weight in BP control |
| $x_m, \mathbf{x}_n, \mathbf{X}$ | m 's queue length, queue length vector of n , queue length vector of network |
| $\epsilon, \mathbf{\epsilon}$ | reserve demand calculated by S-only algorithm, reserve demand vector |
| θ, η | success rate of I-SFR prediction, accuracy of I-SFR prediction |
| $\lambda_m, \mathbf{\lambda}$ | m 's demand arrival rate consisting of exogenous demand and upstream demands, demand arrival rate vector |
| ρ_m | different I-SFR event's probability of m |
| $\Phi_n, \mathbf{\Phi}$ | set of allowable intersection phases at n , set of allowable network phasing schemes: $\mathbf{\Phi} \equiv \times_{n \in \mathcal{N}} \Phi_n$ |
| Φ_n, Φ | an allowable intersection phase at n : $\Phi_n \in \mathbf{\Phi}_n$, an allowable network phasing scheme: $\Phi \subset \mathbf{\Phi}$ and $\Phi \equiv \times_{n \in \mathcal{N}} \Phi_n$ |
| $\phi_m, \mathbf{\phi}$ | m 's passing status (1 if passing is allowed, and 0 otherwise), the vector of passing status of all movements |

In short, although the queue length information may contribute to the prediction accuracy (the occupancy information used in the “nn” method), it does not mean that the prediction error

Table 3: χ^2 test for independence of different movements' I-SFRs.

| Movements | Data sample | Degree of freedom | χ^2 | Critical value ($\alpha = 0.1$) | Critical value ($\alpha = 0.01$) | Description |
|------------------------|-------------|-------------------|----------|-----------------------------------|------------------------------------|---|
| ②-east-T ②-east-L | 634 | 72 | 96.33 | 87.74 | 102.81 | from the same approach |
| ④-south-T ④-south-L | 191 | 30 | 46.90 | 40.26 | 50.89 | |
| ②-north-L ②-south-L | 174 | 36 | 35.18 | 47.21 | 58.62 | at the same intersection |
| ④-north-L ④-north-T | 94 | 16 | 15.18 | 23.54 | 32.00 | |
| ①-north-T ②-north-T | 477 | 16 | 12.59 | 23.54 | 32.00 | from neighboring intersection and with the same direction |
| ③-south-T ④-south-T | 79 | 10 | 6.17 | 15.99 | 23.21 | |

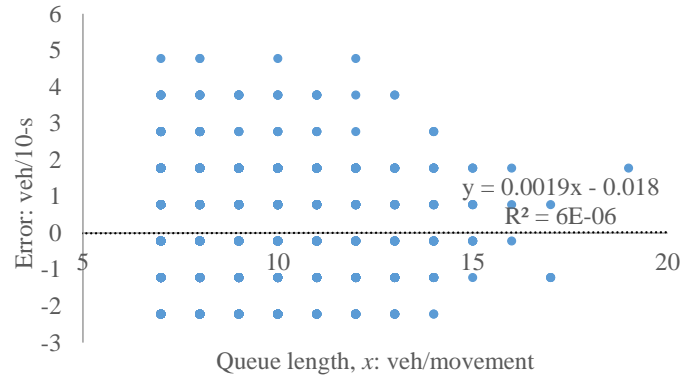
is not independent of queue length. This is common in multiple linear regression. Even if adding a variable can significantly reduce the deviation of prediction error, it does not mean the added variable and the prediction error are dependent.

Appendix 4: Choice of threshold for determining the reserve demand

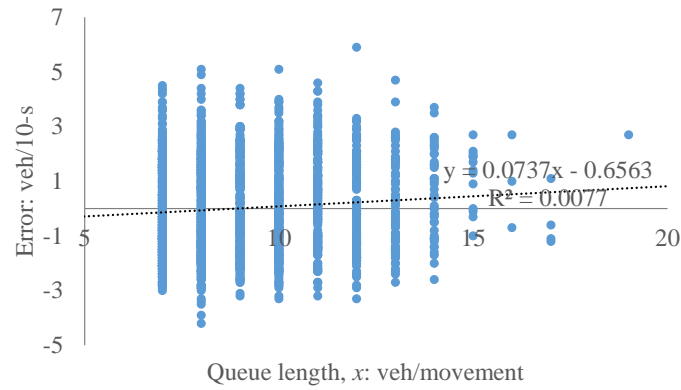
In this appendix, we take BP as an example to show why 100-veh is chosen as the threshold for determining reserve demand. Fig. 18 shows the number of stacked vehicles with the increased demand rate given a fixed random seed.

The curves of staked vehicles include two parts. From 0 to about 100 increased demand rate (about 80 for “mean” and 120 for “nn”), the number of stacked vehicles is about 0, which means the demand is within the ADR. When the increased demand rate is larger than 100, the number of stacked vehicles keeps growing, which means demand is going beyond the ADR. However, it is hard to judge at which moment or stacked-vehicle number the demand exactly reaches the ADR’s upper bound. Despite this, we can find that once the number of stacked vehicles increases, the relative positions of the three curves are stable. Setting the threshold to 100, 200, or 300 vehs makes little difference to the gap between different methods’ reserve demand. Therefore, we choose 100-veh as the threshold as 1) it is big enough to represent that the demand has reached the ADR’s upper bound, and 2) it is not too big and can save simulation time.

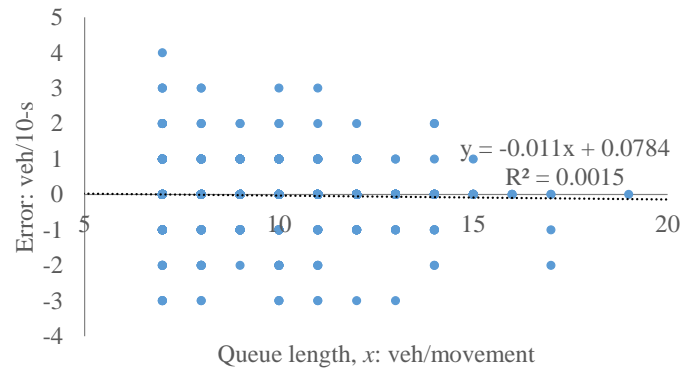
In Fig. 19, we further display the queueing vehicles (sum of queueing lengths for all movements in an approach) in a critical approach (easy to spill back) given the same random seed. Note that a curve’s “platform stage” means the whole approach is blocked, and no vehicles can enter. Because vehicles’ sizes and space headways differ, the vehicle numbers at the “platform stage” could also vary. Once the “platform stage” is reached, no vehicles can pass the intersection (including the right-turns since they are blocked by the through and left-turn vehicles). In general, “est” perform better than “mean” because it arrives at the “platform stage” later. And “nn” performs even better than “est”. This is consistent with the results in Fig. 12 and Fig. 18.



(a) Prediction with “mean” method: the value and significance of Fisher exact test are 87.43 and 0.38 (> 0.05).



(b) Prediction with “est” method: the value and significance of Fisher exact test are 152.42 and 0.16 (> 0.05).



(c) Prediction with “nn” method: the value and significance of Fisher exact test are 105.26 and 0.55 (> 0.05).

Fig. 17: Scatters of errors at movement ①-north-L with 1,854 data samples.

References

Allen, D.P., Hummer, J.E., Rouphail, N.M., Milazzo, J.S., 1998. Effect of bicycles on capacity of signalized intersections. Transportation Research Record 1646, 87–95.

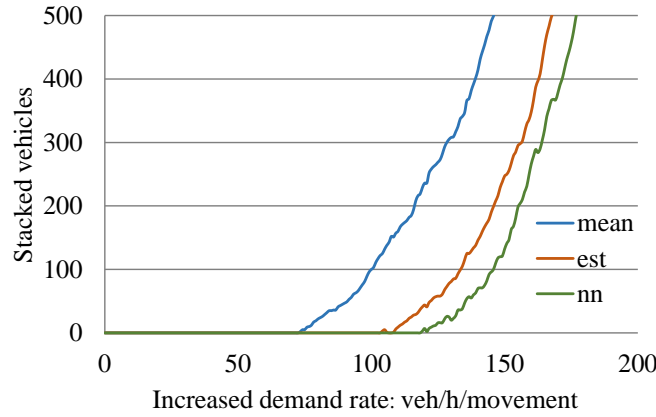


Fig. 18: Stacked vehicle of the network with the increase of demand rate given a random seed.

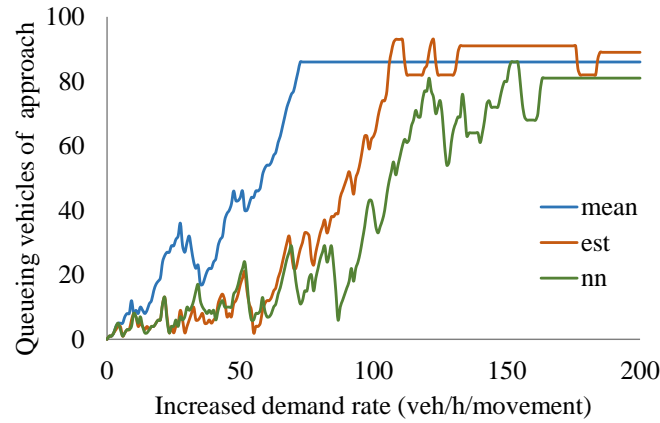


Fig. 19: Queueing vehicles at approach ①-west with increase of demand rate given a random seed.

Barman, S., Levin, M.W., 2022. Performance evaluation of modified cyclic max-pressure controlled intersections in realistic corridors. *Transportation Research Record* 2676, 110–128.

Chai, H., Zhang, H.M., Ghosal, D., Chuah, C.N., 2017. Dynamic traffic routing in a network with adaptive signal control. *Transportation Research Part C: Emerging Technologies* 85, 64–85.

Chen, R., Hu, J., Levin, M.W., Rey, D., 2020. Stability-based analysis of autonomous intersection management with pedestrians. *Transportation Research Part C: Emerging Technologies* 114, 463–483.

Christofa, E., Papamichail, I., Skabardonis, A., 2013. Person-based traffic responsive signal control optimization. *IEEE Transactions on Intelligent Transportation Systems* 14, 1278–1289.

De Gier, J., Garoni, T., Rojas, O., 2011. Traffic flow on realistic road networks with adaptive traffic lights. *Journal of Statistical Mechanics: Theory and Experiment* 2011, P04008.

Dion, F., Hellinga, B., 2002. A rule-based real-time traffic responsive signal control system with transit priority: application to an isolated intersection. *Transportation Research Part B: Methodological* 36, 325–343.

- Dixit, V., Nair, D.J., Chand, S., Levin, M.W., 2020. A simple crowdsourced delay-based traffic signal control. *PLoS one* 15, e0230598.
- Du, Y., Kouvelas, A., 2022. Max-pressure traffic signal control for mixed traffic flow based on capacity estimation, in: 10th Symposium of the European Association for Research in Transportation (hEART 2022).
- Feng, Y., Head, K.L., Khoshmagham, S., Zamanipour, M., 2015. A real-time adaptive signal control in a connected vehicle environment. *Transportation Research Part C: Emerging Technologies* 55, 460–473.
- Gettman, D., Shelby, S., Head, L., Bullock, D., Soyke, N., 2007. Data-driven algorithms for real-time adaptive tuning of offsets in coordinated traffic signal systems. *Transportation Research Record* 2035, 1–9.
- Gregoire, J., Frazzoli, E., De La Fortelle, A., Wongpiromsarn, T., 2014a. Back-pressure traffic signal control with unknown routing rates. *IFAC Proceedings Volumes* 47, 11332–11337.
- Gregoire, J., Qian, X., Frazzoli, E., De La Fortelle, A., Wongpiromsarn, T., 2014b. Capacity-aware backpressure traffic signal control. *IEEE Transactions on Control of Network Systems* 2, 164–173.
- Gregoire, J., Samaranayake, S., Frazzoli, E., 2016. Back-pressure traffic signal control with partial routing control, in: *IEEE 55th Conference on Decision and Control (CDC)*, pp. 6753–6758.
- Hao, S., Yang, L., Ding, L., Guo, Y., 2019. Distributed cooperative backpressure-based traffic light control method. *Journal of Advanced Transportation* 2019.
- He, J., Hou, Z., 2012. Ant colony algorithm for traffic signal timing optimization. *Advances in Engineering Software* 43, 14–18.
- Hurdle, V., 1984. Signalized intersection delay models—a primer for the uninitiated. *Transportation Research Record* 971, 96–105.
- Kouvelas, A., Lioris, J., Fayazi, S.A., Varaiya, P., 2014. Maximum pressure controller for stabilizing queues in signalized arterial networks. *Transportation Research Record* 2421, 133–141.
- Lämmer, S., Helbing, D., 2008. Self-control of traffic lights and vehicle flows in urban road networks. *Journal of Statistical Mechanics: Theory and Experiment* 2008, P04019.
- Lämmer, S., Helbing, D., 2010. Self-stabilizing decentralized signal control of realistic, saturated network traffic (Technical Report No. 10-09-019). Santa Fe Institute.
- Le, T., Kovács, P., Walton, N., Vu, H., Andrew, L., Hoogendoorn, S., 2015. Decentralized signal control for urban road networks. *Transportation Research Part C: Emerging Technologies* 58, 431–450.
- Le, T., Vu, H.L., Walton, N., Hoogendoorn, S.P., Kovács, P., Queija, R.N., 2017. Utility optimization framework for a distributed traffic control of urban road networks. *Transportation Research Part B: Methodological* 105, 539–558.
- Levin, M.W., 2023. Max-pressure traffic signal timing: A summary of methodological and experimental results. *Journal of Transportation Engineering, Part A: Systems* 149, 03123001.

- Levin, M.W., Hu, J., Odell, M., 2020. Max-pressure signal control with cyclical phase structure. *Transportation Research Part C: Emerging Technologies* 120, 102828.
- Li, L., Jabari, S.E., 2019. Position weighted backpressure intersection control for urban networks. *Transportation Research Part B: Methodological* 128, 435–461.
- Li, L., Jabari, S.E.G., 2020. A decentralized network control approach based on continuum traffic flow modeling, in: 99th TRB Annual Meeting. Washington, DC 2020.
- Li, L., Okoth, V., Jabari, S.E., 2021. Backpressure control with estimated queue lengths for urban network traffic. *IET Intelligent Transport Systems* 15, 320–330.
- Lin, D., Jabari, S.E., 2019. Transferable utility games based intersection control for connected vehicles, in: 2019 IEEE Intelligent Transportation Systems Conference (ITSC), IEEE. pp. 3496–3501.
- Lin, D., Jabari, S.E., 2021. Pay for intersection priority: A free market mechanism for connected vehicles. *IEEE Transactions on Intelligent Transportation Systems* 23, 5138–5149.
- Lin, D., Ma, W., Li, L., Wang, Y., 2016. A driving force model for non-strict priority crossing behaviors of right-turn drivers. *Transportation Research Part B: Methodological* 83, 230–244.
- Liu, H., Gayah, V.V., 2022. A novel max pressure algorithm based on traffic delay. *Transportation Research Part C: Emerging Technologies* 143, 103803.
- Liu, H., Gayah, V.V., 2023. Total-delay-based max pressure: A max pressure algorithm considering delay equity. *Transportation Research Record* , 03611981221147051.
- Mercader, P., Uwayid, W., Haddad, J., 2020. Max-pressure traffic controller based on travel times: An experimental analysis. *Transportation Research Part C: Emerging Technologies* 110, 275–290.
- Milazzo, J.S., Roupail, N.M., Hummer, J.E., Allen, D.P., 1998. Effect of pedestrians on capacity of signalized intersections. *Transportation Research Record* 1646, 37–46.
- Neely, M., 2010. Stochastic network optimization with application to communication and queueing systems. *Synthesis Lectures on Communication Networks* 3, 1–211.
- Neely, M., Modiano, E., Rohrs, C., 2005. Dynamic power allocation and routing for time-varying wireless networks. *IEEE Journal on Selected Areas in Communications* 23, 89–103.
- Noaeen, M., Mohajerpoor, R., Far, B.H., Ramezani, M., 2021. Real-time decentralized traffic signal control for congested urban networks considering queue spillbacks. *Transportation Research Part C: Emerging Technologies* 133, 103407.
- Papageorgiou, M., Diakaki, C., Dinopoulou, V., Kotsialos, A., Wang, Y., 2003. Review of road traffic control strategies. *Proceedings of the IEEE* 91, 2043–2067.
- Rey, D., Levin, M.W., 2019. Blue phase: Optimal network traffic control for legacy and autonomous vehicles. *Transportation Research Part B: Methodological* 130, 105–129.
- Robbennolt, J., Chen, R., Levin, M., 2022. Microsimulation study evaluating the benefits of cyclic and non-cyclic max-pressure control of signalized intersections. *Transportation Research Record* 2676, 303–317.

- Smith, M., 1980. A local traffic control policy which automatically maximises the overall travel capacity of an urban road network. *Traffic Engineering & Control* 21, HS-030 129.
- Smith, M., 2011. Dynamics of route choice and signal control in capacitated networks. *Journal of Choice Modelling* 4, 30–51.
- Sun, X., Yin, Y., 2018. A simulation study on max pressure control of signalized intersections. *Transportation Research Record* 2672, 117–127.
- Tassiulas, L., Ephremides, A., 1992. Stability properties of constrained queueing systems and scheduling policies for maximum throughput in multihop radio networks. *IEEE Transactions on Automatic Control* 37, 1936–1948.
- Transportation Research Board, 2010. Highway Capacity Manual. National Research Council, Washington, DC, USA.
- Tsitsokas, D., Kouvelas, A., Geroliminis, N., 2021. Efficient max-pressure traffic signal control for large-scale congested urban networks, in: 21st Swiss Transport Research Conference (STRC 2021), STRC.
- Varaiya, P., 2013. Max pressure control of a network of signalized intersections. *Transportation Research Part C: Emerging Technologies* 36, 177–195.
- Wang, X., Yin, Y., Feng, Y., Liu, H.X., 2022. Learning the max pressure control for urban traffic networks considering the phase switching loss. *Transportation Research Part C: Emerging Technologies* 140, 103670.
- Wang, Y., Rong, J., Zhou, C., Gao, Y., 2020. Dynamic estimation of saturation flow rate at information-rich signalized intersections. *Information* 11, 178.
- Wei, H., Chen, C., Zheng, G., Wu, K., Gayah, V., Xu, K., Li, Z., 2019. Presslight: Learning max pressure control to coordinate traffic signals in arterial network, in: *Proceedings of the 25th ACM SIGKDD International Conference on Knowledge Discovery & Data Mining*, pp. 1290–1298.
- Wongpiromsarn, T., Uthacharoenpong, T., Wang, Y., Frazzoli, E., Wang, D., 2012. Distributed traffic signal control for maximum network throughput, in: *15th International IEEE Conference on Intelligent Transportation Systems (ITSC)*, pp. 588–595.
- Wu, J., Ghosal, D., Zhang, M., Chuah, C.N., 2017. Delay-based traffic signal control for throughput optimality and fairness at an isolated intersection. *IEEE Transactions on Vehicular Technology* 67, 896–909.
- Xiao, N., Frazzoli, E., Li, Y., Luo, Y., Wang, Y., Wang, D., 2015a. Further study on extended back-pressure traffic signal control algorithm, in: *2015 54th IEEE Conference on Decision and Control (CDC)*, IEEE. pp. 2169–2174.
- Xiao, N., Frazzoli, E., Li, Y., Wang, Y., Wang, D., 2014. Pressure releasing policy in traffic signal control with finite queue capacities, in: *IEEE 53rd Annual Conference on Decision and Control (CDC)*, pp. 6492–6497.
- Xiao, N., Frazzoli, E., Luo, Y., Li, Y., Wang, Y., Wang, D., 2015b. Throughput optimality of extended back-pressure traffic signal control algorithm, in: *2015 23rd Mediterranean Conference on Control and Automation (MED)*, IEEE. pp. 1059–1064.

- Xu, T., Barman, S., Levin, M.W., Chen, R., Li, T., 2022. Integrating public transit signal priority into max-pressure signal control: Methodology and simulation study on a downtown network. *Transportation Research Part C: Emerging Technologies* 138, 103614.
- Zaidi, A., Kulcsar, B., Wymeersch, H., 2015. Traffic-adaptive signal control and vehicle routing using a decentralized back-pressure method, in: 2015 European Control Conference (ECC), pp. 3029–3034.
- Zaidi, A., Kulcsár, B., Wymeersch, H., 2016. Back-pressure traffic signal control with fixed and adaptive routing for urban vehicular networks. *IEEE Transactions on Intelligent Transportation Systems* 17, 2134–2143.
- Zhao, J., Li, P., Zheng, Z., Han, Y., 2018. Analysis of saturation flow rate at tandem intersections using field data. *IET Intelligent Transport Systems* 12, 394–403.